Department of Mechanical Engineering
Energy Technology Research Group

Ecovat Nederland B.V.

Peak Buffering by the Ecovat Thermal Energy Storage System

Master Thesis

M.M.M.M. (Marijn) van den Heuvel

Supervisors:
prof.dr.ir. D.M.J. Smeulders
ir. L.A.J. Mazairac

Committee:
prof.dr.ir. D.M.J. Smeulders
dr.ir. C.C.M. Rindt
dr. G. Finotello
ir. L.A.J. Mazairac (advisor)

Veghel, Wednesday 7$^{\text{th}}$ October, 2020

Abstract

The rise of sustainable energy sources introduces a temporal mismatch on a daily and seasonal basis; therefore, energy storage plays an important role. Ecovat B.V. offers such storage by means of a thermal energy storage tank. The Ecovat storage tank is a large-scale underground tank that stores heat on a seasonal basis using water as storage fluid. However, Ecovat desires to extend the applicability of the Ecovat storage tank, from seasonal storage towards a peak buffer but is uncertain about its technical limits. Therefore, additional research is required regarding the suitability of the Ecovat storage tank as a peak buffer. In doing so, existing systems that include seasonal- and peak buffer tanks are compared. Based on this comparison, two use cases are designed, one seasonal and one buffer use case. These use cases are inserted into a convex optimisation model, which returns the costs optimised operation. The operation of the tank as seasonal- and buffer storage is compared using the cycle number, storage efficiency, equivalent CO_2 emissions, and total annual costs. This comparison shows that the Ecovat storage tank reduces the equivalent CO_2 emissions, but increases the annual costs for both use cases compared to when natural gas is used to supply the heat demand. Moreover, it is observed that the buffer use case results in a higher storage efficiency and 6.5 times higher cycle number than the seasonal use case. Therefore, it is concluded that the Ecovat storage tank is suitable as buffer storage with a CN of 9.42 [-], which approaches a monthly discharged buffer tank.

Contents

List of Figures

List of Tables

Nomenclature

Symbol	Description	Unit
A	Area	m^2
$\boldsymbol{b}$	Budget values	-
c	Costs	€
c_p	Specific heat	kWh/(kg K)
d	Diameter	m
E	Energy	kWh
f	Objective function	-
$\boldsymbol{g}$	Governing equations	-
G	Irradiance	kWh/m^2
GP	Gas profile	-
h	Height	m
k	Optimisation iteration	-
m	Mass	kg
$\dot{m}$	Mass flow	kg/s
P	Power	W
Q	Heat	kWh
q	Heat transfer	W
R	Thermal resistance	m^2K/W
RER	Heating temperature regression coefficient	$1/°C$
t	Time	hr
T	Temperature	°C
TOP	Temperature independent gas profile	-
U	Overall heat transfer coefficient	$W/(m^2K)$
V	Volume	m^3
$\boldsymbol{x}$	Optimisation variables	-
Greek		
α	Optimisation parameter	-
δ	Auxiliary multiplier	-

Δ	Difference	-
ε	Equivalent CO_2 emissions	kg
η	Storage efficiency	-
κ	Thermal conductivity	W/(m K)
λ	Lagrangian multiplier	-
ρ	Density	kg/m^3
ϕ	Period state parameter	-

Indices/Subscripts

diff	Difference
e	Electrical
init	Initial
m	Number of periods
max	Maximum
min	Minimum
n	Number of layers
term	Terminal
th	Thermal
w	Water

Acronyms

ADMM	Alternating Direction Method of Multipliers
AWHP	Air-Water Heat Pump
Capex	Capital Expenditure
CHP	Combined Heat and Power
CN	Cycle Number
COP	Coefficeint of Performance
EPS	Expanded Polystyrene
FHP	Flexible Heat and Power
GHG	Greenhouse Gas
HP	Heat Pump
KPI	Key Performance Indicator
NDC	Nationally Determined Contributions
Opex	Operational Expenses
PDHU	Pimlico District Heating Undertaking
TTES	Tank Thermal Energy Storage
UNFCCC	United Nations Framework Convention on Climate Change
WWHP	Water-Water Heat Pump

Chapter 1

Introduction

The Paris Agreement was introduced in 2015, during the 21st Conference of the Parties of the United Nations Framework Convention on Climate Change (UNFCCC). This agreement stated that the global temperature rise this century must be kept below 2 [°C] compared to pre-industrial levels. Furthermore, all 196 parties should pursue to limit the temperature increase even further, to a maximum temperature rise of 1.5 [°C]. The Paris Agreement requires all parties to put forward their best efforts by means of nationally determined contributions (NDCs) (United Nations, 2015). The success of the Paris Agreement thus relies heavily on the actions of each of the respective parties. The member states of the European Union signed the Paris Agreement in 2016, which led to the individual climate laws for each member state. The Dutch government agreed upon one of the most ambitious climate laws of all members. The goal is to reduce its greenhouse gas (GHG) emissions by 49 [%] in 2030 and 95 [%] in 2050, both compared to the measured GHG emissions of the Netherlands in 1990. In reaching these goals, significant efforts must be made to save energy and increase the share of renewable energy in the energy mix (Ministerie van Economische Zaken, 2016). Additionally, a social aspect is related to the rise in sustainable energy sources in the Netherlands. Currently, a substantial amount of residential heating, in the form of gas, is provided by the gas fields located in the province of Groningen. The extraction of gas has resulted in numerous earthquakes, leading to multiple lawsuits supported by at least 3,500 victims. An estimated 100,000 houses have together lost an estimated 1 billion [€] in value due to seismic activity as a direct result of the gas extraction. The Dutch government started taking actions back in 2014 to reduce the extraction of natural gas from these fields to zero by 2030. However, this goal got recently updated to 2022, pushing the rise of sustainable energy sources even further (Boffey, 2018).

With the above two described reasons as main incentives, the rise of sustainable energy sources is set. These sustainable energy sources generally depend on variable sources, e.g. wind and solar, which introduce new challenges. One major challenge is the fluctuations on a daily and seasonal basis, causing a temporal mismatch between sustainable energy availability and demand. Therefore, energy storage plays an important role. Ecovat Nederland B.V. offers such storage by means of a thermal energy storage tank. It operates by inserting thermal energy in the form of high-temperature water, into a large-volume underground tank, which charges the tank with heat. Ecovat retains this heat for some time, and when there is a demand for it, the heat is discharged to consumers by a heat grid.

1.1 Problem Identification

The Ecovat storage tank is entirely designed to bridge the gap between the seasonal energy mismatch. Its design consists of pre-fabricated concrete wall parts, which are stacked on each other in a cylindrical form, as visualised in Figure 1.1(a). The standardised parts allow creating different sized tanks and to design the best-suited tank for each individual case. Furthermore, the tank is radially insulated by foam glass, a concrete filling, and a constructive soil mix wall, respectively. The top of the tank is closed with triangular concrete parts, as shown in Figure 1.1(b). These triangular parts are then insulated by foam glass, expanded polystyrene (EPS), and finally covered up with soil. The bottom of the tank is a cast concrete floor with no additional insulation added.

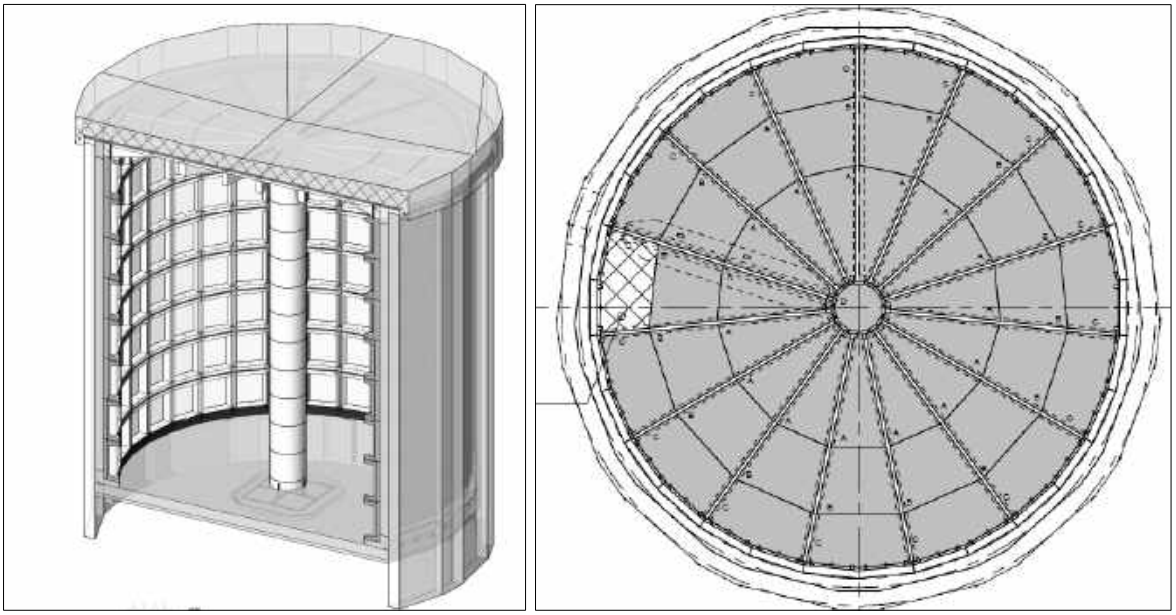

(a) (b)

Figure 1.1: (a) Cross-section of the cylindrical Ecovat storage tank, with the pre-fabricated concrete wall parts clearly visible. (b) Triangular concrete parts forming the top of an Ecovat storage tank.

One version of this Ecovat storage tank has been successfully constructed in Uden, the Netherlands, see Figure 1.2. This storage tank is roughly 11 [m] in diameter and has a height of 16 [m]. It was set into operation in 2017 and successfully demonstrated the proof-of-concept. Nowadays, it is mainly used for gathering experimental data about the Ecovat storage tank for further development. This version of the Ecovat storage tank is a closed tank system, meaning that in this version's design, no water is directly flowing into or out of the storage tank due to the heat exchangers being cast in the walls. After this first built in Uden, new insights have been gathered, and Ecovat decided to change towards an open tank system design. In this open tank system design, radial diffusers are present which deal with the exchange of heat by injecting hot water into and extracting cold water from the storage tank.

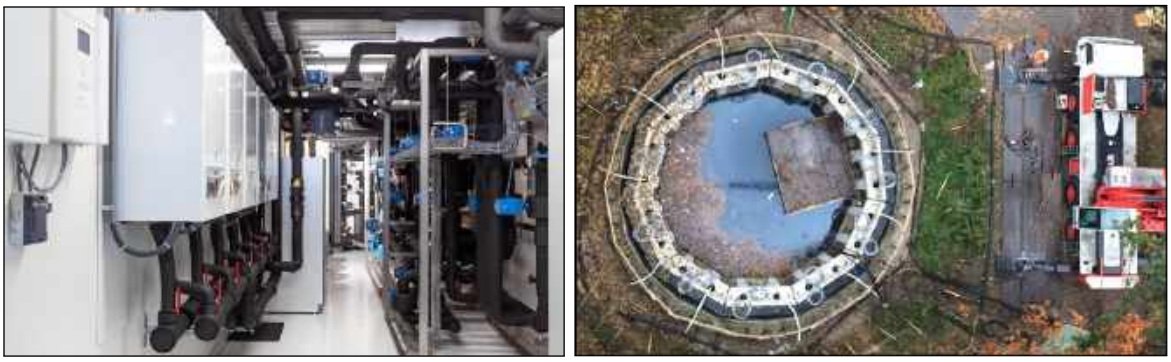

(a) (b)

Figure 1.2: (a) Installation of the technical room on top of the Ecovat storage tank in Uden. This room contains the heat pumps, controlling software, and piping from and to the tank. (b) Ecovat storage tank in Uden under construction. At this stage the tank it is still missing its insulated top.

The Ecovat storage tank is only designed to serve as a seasonal energy storage system. However, from industry, there is a request to completely charge and discharge the Ecovat storage tank more often during the year, preferably even on a day-to-night basis. This functioning as a peak buffer is not yet researched for an Ecovat storage tank. Besides, from an internally conducted research, it became apparent that the capital expenditure (Capex) of an Ecovat storage tank is rather high compared to other seasonal thermal energy systems (de Groot, 2020). Extending the applicability of the Ecovat storage tank, from the conventional seasonal storage towards the desired peak buffer, requires additional research. In doing so, a set of sub-research questions is proposed leading to a defined main research question when combined.

1.2 Problem Definition & Research Questions

In the problem identification, it is mentioned that additional research has to be conducted to state something meaningful about the Ecovat storage tank and its limitations. This results in the following problem definition:
Ecovat desires to extend the applicability of the Ecovat storage tank, from the conventional seasonal storage towards a peak buffer, due to several requests from industry. However, Ecovat is uncertain about the technical limits of their storage tank. Therefore, not knowing if, or to which extent, it is suitable as a peak buffer.

Based on this problem definition, the main research question for this study is defined as follows:
How suitable is it, financially and technically, to use the Ecovat seasonal heat storage system as peak buffer heat storage?

In order to find an answer to the main research question, three sub-research questions are introduced:

1. What are similarities and differences of typical peak buffer heat storage and seasonal heat storage systems?
A comparison study is performed based on literature in chapter 2 to create an overview of existing tank thermal energy storage systems. Focusing on heat sources, heat demand, and tank characteristics, this overview points out similarities and differences for two classifications of storage tanks, seasonal and peak buffer.

2. What are possible use cases for the Ecovat storage tank while using it a peak buffer storage?
Two use cases are designed in chapter 3 based on the comparison made in the first research question, resulting in one seasonal and one peak buffer use case. The use cases include heat sources, heat demand, and tank characteristics similar to existing systems to represent reality as close as possible. The purpose of these use cases is to use as input for a model and compare the Ecovat storage tank performance for both situations.

3. Considering different charging and discharging strategies of use cases, which case would be optimal for the Ecovat energy storage?
Relevant equations for the Ecovat storage tank are explained and modelled in chapter 4. To consider optimal charging and discharging strategies, this model is expanded to an optimisation model, which takes the designed use cases as input. The optimisation model is validated with experimental data obtained from the Ecovat storage tank in Uden. The purpose of this model is to result in the optimised annual performance for both the seasonal- and buffer use case and compare it based on different performance indicators, which is presented in chapter 5.

Chapter 2

Typical Water-Based Tank Thermal Energy Storage Systems

Several types of thermal energy storage exist, so-called latent, sorption, and sensible heat storage. The former stores heat in the phase change of a material, the second stores heat through physical or chemical bonding, and the latter changes the temperature of a liquid or solid to store or release heat. In practice, sensible heat storage is the most widely applied type of thermal energy storage. The most common variants of sensible heat storage are:

- Aquifer thermal energy storage (ATES);
- Borehole thermal energy storage (BTES);
- Cavern thermal energy storage (CTES);
- Pit thermal energy storage (PTES);
- (Underground) Tank thermal energy storage (TTES) (Bott et al., 2019).

In the current study, it is decided to exclusively focus on closed artificial tank storage systems in which water is used as storage fluid. This type is most similar to the Ecovat storage tank. The first large-scale TTES was built back in 1950 when the Pimlico District Heating Undertaking (PDHU) was founded in the heart of London. At that moment in time, a vast amount of coal-fired power plants were present in London, causing smog problems. A storage tank was built to cut emissions drastically (PDHU, 2017). Nowadays, there are numerous TTES systems in use, and more to come. The majority of these systems are located in Germany as a result of the dedicated research programs, Solarthermie-2000 (1993 - 2002) and Solarthermie2000-plus (2004 - 2008) (Bott et al., 2019).

In the current chapter, two types of TTES system are treated, seasonal- and buffer TTES systems. In section 2.1, three representative seasonal TTES systems are introduced. In section 2.2, a closer look into peak buffer storage systems is given. System components that are described include storage tank characteristics, heat sources as well as the heat demand, as visualised in Figure 2.1. The chapter is concluded by a comparison regarding similarities and differences of typical peak buffer heat storage and seasonal heat storage.

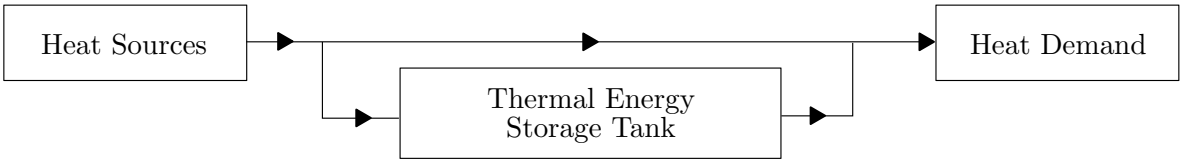

Figure 2.1: Schematics of described components for systems included in the comparison.

2.1 Seasonal TTES Systems

The presence of seasonal TTES systems is not uncommon any more. In past decades, many new systems have gone into operation. According to Bott et al. (2019), fourteen seasonal TTES systems were known to be in use in 2019. Three seasonal TTES systems that are deemed to be representative of the collective are described in the following subsections.

2.1.1 Friedrichshafen

The seasonal storage in Friedrichshafen, Germany, started as pilot storage in 1996. The 12,000 [m^3] underground storage tank is constructed from reinforced, pre-stressed concrete and is lined with watertight 1.2 [mm] stainless steel sheets. Only the roof and vertical walls of the tank are insulated. The storage tank provides energy for two residential zones with a total heating area of 39,500 [m^2]. The first residential zone consists of 280 apartments and a daycare. This zone includes 2,700 [m^2] of flat plate solar collectors to generate heat. The second residential zone, added in 2004, includes another 110 dwellings and an extra 1,350 [m^2] of solar collectors. In addition, two gas boilers were added to cover the energy demand for periods when insufficient energy is available from the solar collectors and thermal storage (Mangold & Peuser, 2003; Mangold, 2006). The district heating system, including the storage tank, is visualised in Figure 2.2.

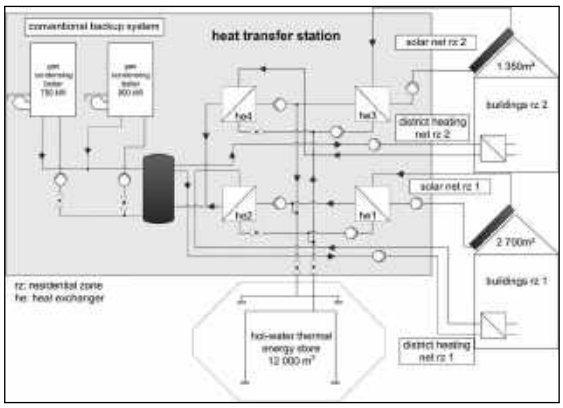

(a)

(b)

Figure 2.2: (a) Schematic of the solar assisted district heating system in Friedrichshafen with a 12,000 [m^3] underground storage tank. This system provides a total heating area of 39,500 [m^2]. The heat in the system is generated via 4,050 [m^2] solar collectors and a conventional backup system with two gas boilers (Bauer et al., 2010). (b) The storage tank in Friedrichshafen while under construction (Solaris, n.d.).

2.1.2 Hanover

The seasonal storage tank in Hanover, Germany, was put into operation in 2000, with a different concept applied from that in Friedrichshafen. In Hanover, no liner is used; instead, the walls are made of high density reinforced concrete (Mangold, 2007). The tank has a volume of 2,750 [m^3], a heat capacity of 160 [MWh], and storage efficiency of 71.2 [%]. It is connected to a district heating system providing heat to 106 dwellings in low energy multi-family buildings, i.e. providing heat to a living area of 7,365 [m^2]. Moreover, within the system, a total area of 1,473 [m^2] of flat plate solar collectors is present to generate the heat. If the solar collectors and storage tank are not able to satisfy the heat demand, heat from a nearby combined heat and power (CHP) plant is used to supply additional heat into the system (Raab et al., 2005). A visualisation of the system is presented in Figure 2.3.

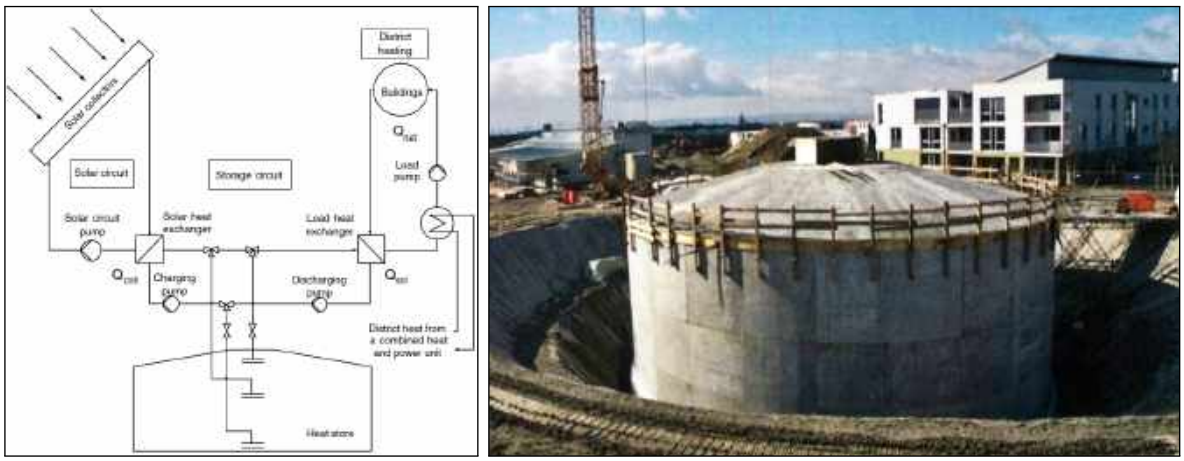

(a) (b)

Figure 2.3: (a) Schematic of the district heating system in Hanover with a 2,750 [m^3] underground storage tank. This system provides heat to 106 dwellings in low energy multi-family buildings with a total heating area of 7,365 [m^2]. The heat in the system is generated via 1,473 [m^2] solar collectors. If necessary, heat from a nearby CHP is supplied into the system when the solar collectors and storage tank are not able to serve the heat demand (Raab et al., 2005). (b) The storage tank in Hanover while under construction (Solaris, n.d.).

2.1.3 Munich

The storage system in Munich, Germany, was put into operation in 2007. The storage tank consists out of two truncated cones, one at the top and one at the bottom, with a 10 [m] high cylinder in between. This cylinder is made by placing pre-fabricated concrete sections with a stainless steel liner at the inner surface in a cylindrical shape. This geometry with truncated cones approaches the form of a sphere giving an optimal area-to-volume ratio for minimising the heat losses (Mangold, 2006). This 5,700 [m^3] tank has a heat capacity of 330 [MWh]. The tank is partially dug into the ground, and its remainder is covered with soil. Such that additional insulation is gained and no space is wasted by creating a recreational area. The district heating system consists of four large blocks of flats and eight smaller townhouses with a total of 319 dwellings and a total heating area of 30,400 [m^2]. The system is for 45 [%] solar-

powered by the collectors on top of the dwellings in Ackermannbogen. The remainder of the demand is covered by the district heating Stadtwerke München (sdg21, 2016). A visualisation of the district heating system in Munich is presented in Figure 2.4.

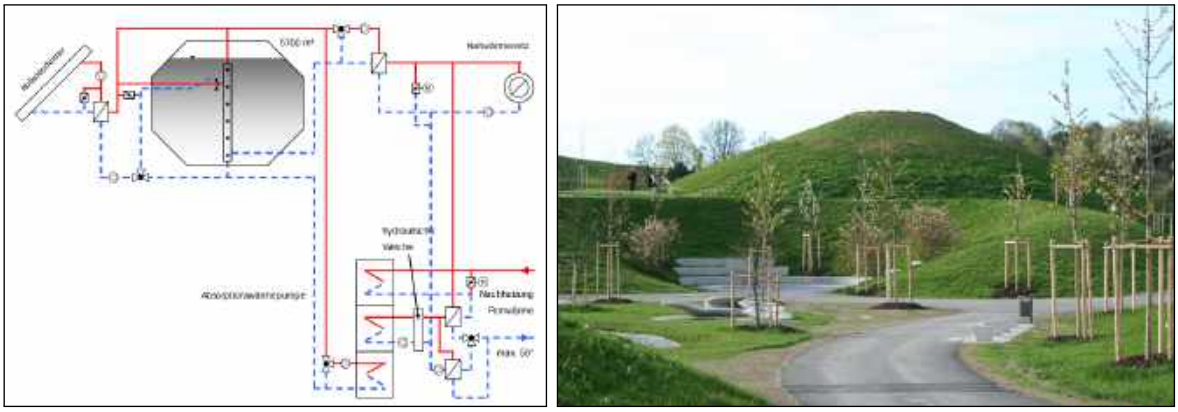

(a) (b)

Figure 2.4: (a) Schematic of the solar assisted district heating system in Munich with a 5,700 [m^3] storage tank. This system provides heat to 319 dwellings and a total heating area of 30,400 [m^2]. The heat in the system is for 45 [%] generated via solar collectors, the remainder of the necessary heat demand is covered by Stadtwerke München (Ochs, 2013). (b) Recreational area in Munich covering the 5,700 [m^3] storage tank below it (Solaris, n.d.).

2.2 Large-Scale Buffer TTES Systems

A distinction is recognised in the broad range of available peak buffer tanks. On one side, it is observed that the majority of large storage tanks used as peak buffers are located near a power plant, e.g. Theiß, Duisburg, or Linz. These locations are beneficial due to the amount of available residual heat. In fact, the first large-scale storage tank was built near the Battersea Power Plant, the PDHU in London, shown in Figure 2.5 (PDHU, 2017). On the other hand, medium-sized peak buffer tank systems designed for smaller neighbourhoods also exist. Both types of existing peak buffer systems are discussed in further detail in the following subsections, using representative system examples.

2.2.1 Theiß

At the EVN Power Plant Theiß near Krems, Austria, a storage tank with a volume capacity of 50,000 [m^3] is in operation, making it one of the biggest buffer storages of Europe (Oberhammer & Prawits, 2012). Worth noting is the fact that use is made of a former oil tank, which is re-constructed and insulated with 300-500 [mm] Rockwool. The heat storage tank near the EVN power plant provides heat for over 5,000 households in the neighbouring regions (EVN, n.d.). The tank is charged and discharged by two diffusers, one at the top and one at the bottom. These diffusers are designed using the principles introduced in Leitner (2013).

(a) (b)

Figure 2.5: PDHU storage tank located in London in (a) 1950 (PDHU, 2017) and (b) 2010 (Vincent-Rous, 2010).

2.2.2 Duisburg

The city of Duisburg, Germany, has recently changed its energy policy, leading to the closing of the coal-powered plant at the start of 2018. A new CHP with gas and steam-powered turbines replaced the old power plant. The peak buffer tank uses a two-phase storage principle, requiring that the storage volume is separated by an insulated roof into an upper and lower zone, as shown in Figure 2.6. These two zones are connected by piping. In the upper zone, warm water is present with a temperature between 60 - 90 [°C], which uses its weight to pressurise the lower zone. This pressure enables the lower zone to reach a temperature exceeding 100 [°C]. The combined volume of the zones is $\approx$43,000 [m^3] and has a total heat capacity of 1,450 [MWh] (Stadtwerke-Duisburg, n.d.). The CHP plant, including the two-phase storage tank, is shown in Figure 2.7(a).

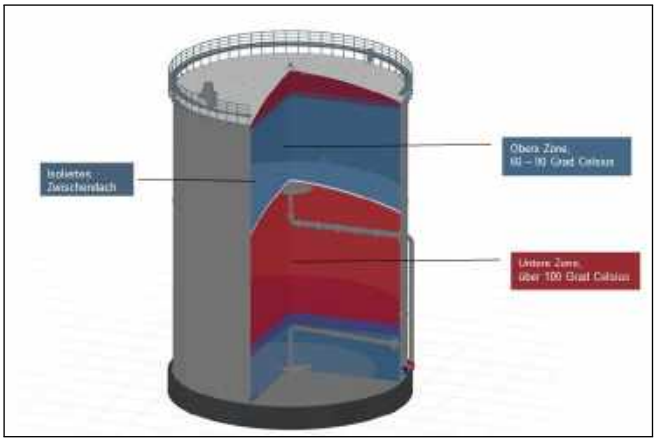

Figure 2.6: Schematic of the inside of the two-phase storage tank in Duisburg. Showing the upper zone, insulated separation, and the high temperature lower zone in the tank (Stadtwerke-Duisburg, n.d.).

2.2.3 Diemen

Only a handful of buffer storage tanks are in operation in the Netherlands. One of the larger tanks is the peak buffer of Vattenfall near the CHP in Diemen. A picture of this tank is provided in Figure 2.7(b). Residual heat, provided by power plants Diemen 33 & 34, is used to supply heat to 75,000 households in Amsterdam, Amstelveen and Almere. A maximum temperature of 125 [°C] can be reached within the tank due to the tank being pressurised at 2.7 [bar]. This high temperature is desired due to the large distances within the district heating system, e.g. the distance covered from the CHP in Diemen to Almere is 8.5 [km]. At which, the high energy water from the tank reduces the required pump power (Automatie-PMA, 2016). The tank itself is made from 37 [mm] steel which is covered by a layer of 500 [mm] of insulation (Vattenfall, n.d.).

2.2.4 Linz

Linz AG, the leading utility company in Upper Austria, put two power station units into operation back in 1970 forming the Linz-Mitte Power Station. During the modernisation of this plant in the early 2000s, a hot water storage tank was added to the system, shown in Figure 2.7(c). The tank has a height of 65 [m] and a diameter of 26 [m], resulting in a total volume of 34,500 [m^3]. It is made out of boiler plating and is welded on site. At the outside of the boiler plating, a layer of 500 [mm] insulation is added. The tank operates at atmospheric pressure with a steam cushion on top to prevent the ingress of air. It is designed for weekly operation, the tank is charged during the week with residual heat from the power plant with a feed temperature of 97 [°C], and is discharged to the district heating system during the weekends. The return temperature of the district heating water equals around 57 - 60 [°C], resulting in a maximum capacity of $\approx$1,300 [MWh]. The storage tank is charged and discharged by water which is injected and extracted by fixed diffusers (Gimmelsberger, 2004).

2.2.5 Angeli di Rosora

The Leaf Community was built in 2008 as a part of the International Energy Agency (IEA) Task 40. The Leaf Community exists of only six apartments divided over three Leaf Houses and another 6,000 [m^2] building, the LeafLab. The community is located in Angeli di Rosora, Italy, and includes a water tank with a volume capacity of 400 [m^3] (Comodi et al., 2015). The storage tank is buried and insulated with 16 [cm] of extruded polystyrene. The thermal storage is charged during weekends using the excess production of PV energy available within the Leaf Community. This excess electricity is used to generate heat by means of heat pumps, which are activated from 8:00 to 16:00 in winter and from 7:00 to 18:00 in summer (Kolokotsa et al., 2019).

(a) (b)

(c)

Figure 2.7: (a) Combined heat and power plant of Stadtwerke Duisburg, including a two-phase thermal energy storage tank. This tank is the grey and white cylindrical tower in the center of the image (Bilfinger SE, 2014). (b) The peak buffer tank located in Diemen while under construction. At this stage the tank is welded but not yet insulated (Lousberg, 2014). (c) Linz AG power station. The grey tower on the left hand side of the image is a 65 [m] high buffer tank. (Linz AG, n.d.).

2.3 Comparison

Taking a look at the aforementioned thermal energy storage systems, several similarities and differences are observed. Some key characteristics of the presented storage tanks are included in Table 2.1.

Table 2.1: Summary of key characteristics for different types of storage tanks.

Name	Type	Year	Volume [m^3]	Height [m]	Diameter [m]	h/d [-]
Friedrichshafen	Seasonal	1996	12,000	20	32	0.63
Hannover	Seasonal	2000	2,750	11	19	0.58
Munich	Seasonal	2007	5,700	10 (16 m)	26	-
London	Buffer	1950	2,500	39	9	4.33
Linz	Buffer	2004	34,500	65	26	2.50
Theiß	Buffer	2008	50,000	30	50	0.60
Diemen	Buffer	2015	22,000	50	26	1.92
Duisburg	Buffer	2018	43,000	44	36	1.22

The first property that shows a difference in design between seasonal- and buffer storages is the height-over-diameter ratio (h/d-ratio). From Table 2.1, it is observed that seasonal tanks have ratios less than 1.0 [-] where buffer tanks mainly have ratios higher than 1.0 [-]. The difference in this ratio is explained based on findings obtained from numerous experiments and simulations. The optimal h/d-ratio for a seasonal storage tank, given 1.2 - 1.6 cycles per year, equals $\approx$1.0 [-]. The main reason being that this ratio gives an optimal area-to-volume ratio (A/V-ratio), minimising the conductive losses for a longer storage time. The optimal h/d-ratio for a buffer storage tank with 260 - 280 cycles per year equals $\approx$3.0 [-] (Ochs, 2013), which is explained by the effects of mixing. To charge and discharge the tank more, as is the case for buffer storage systems, higher flow rates are necessary. The increase in flow rate increases the mixing of water, which is undesired as this reduces the efficiency of a storage tank. However, this mixing is not only influenced by the flow rate but also by the h/d-ratio. Simulations show that increasing the h/d-ratio from 1.0 [-] to 3.8 [-], decreases mixing by 30.0 [%], thus compensating for the efficiency losses from higher flow rates (Karim et al., 2018). Note that the summary of Table 2.1 shows that non-ideal ratios are used in reality due to economic considerations.

The second difference is the primary tank material. From the storage tanks in Friedrichshafen (subsection 2.1.1), Hanover (subsection 2.1.2), and Munich (subsection 2.1.3), it is observed that for seasonal heat storages, concrete is used as the primary material, which is either high-quality concrete or concrete with a stainless steel liner. For the buffer tanks in Linz (subsection 2.2.4), Theiß (subsection 2.2.1), and Diemen (subsection 2.2.3), mostly steel is used. This steel is then insulated at the outside of the tank. The aforementioned difference is directly related to the third difference, buried versus above-ground tanks. It is observed that seasonal storages are often placed underground or partially underground and then covered with soil, thus eliminating convective heat losses from ambient air. On the contrary, most of the large-tank buffers are located above ground. The choice of specific

materials and their placing location is based on the material characteristics of both concrete and steel. According to a distributor in storage tanks in the United States, steel tanks are designed to withstand the underground pressure. However, due to the steel tank being underground, it becomes susceptible to rust and corrosion. Such problems are more difficult to detect and recover underground, compared to conventional above-ground tanks (GoToTanks, Inc., 2018). On the contrary, concrete is not favourable above ground due to concrete being particularly strong under compression but weak under tension. The head of the water creates tension on the lower parts of the concrete construction, thus making it non-ideally loaded.

In addition to these differences, there are also some similarities. First, the volume of both seasonal- and buffer storage tank is based on the supply and demand for heat. The available heat is considered as well as the desired heat capacity to fulfil the heat demand for a given amount of dwellings. It is observed that small-volume buffer tanks are used within smaller district heating systems where only a limited amount of heat is available, e.g. due to limited space for solar collectors. Additionally, there are high volume buffer storages which are located near power plants having sufficient residual heat to serve a large amount of heating area. However, there is a limit to this dependency for seasonal storage systems. Mangold (2007) states that seasonal thermal storage is only attractive if the volume surpasses 1000 [m^3] because smaller seasonal storage tanks are too inefficient due to the A/V-ratio resulting in high heat losses.

In the comparison, differences and similarities are presented. It is found that the h/d-ratios for seasonal storages are less than 1.0 [-] whereas buffer tanks have h/d-ratios higher than 1.0 [-]. Both h/d-ratios are based on the efficiencies and costs for their designed operation. Furthermore, it is observed that seasonal storage tanks are made out of concrete and located underground, whereas buffer tanks are generally made from steel and placed above-ground. This placing is explained by the material properties of both concrete and steel. Next to these differences, a tank characteristic that is similar for both types of storage tanks relates to the heat capacity. The heat capacity of a tank is based on the available heat sources, i.e. a high amount of residual heat or a limited number of solar collectors, and the desired heat demand.

Chapter 3

Seasonal- and Buffer Use Cases

Various use cases are designed, representing real-time scenarios. These use cases are modelled to see which charging and discharging strategy is preferred when using the Ecovat storage tank. An in-depth description of the use case is given in section 3.1, which is finalised with an overview in section 3.2. The indicators used to compare the different use cases are presented in section 3.3.

3.1 Use Case Description

Two types of use cases are designed within this chapter, one representing a seasonal case and one buffer case. The use cases consist out of multiple system components with the Ecovat storage tank as the main component, visualised in Figure 3.1. Both use cases include the same system components; however, the amount by which a component is included differs. The heat sources included in the use cases are heat pumps, solar collectors and residual heat from the neighbouring industry. The total heat demand consists of the combined heat demand from a number dwellings. The heat losses for the use cases only relate to the heat losses from the tank. Each of the individual components is treated in-depth in subsections 3.1.1 - 3.1.3.

3.1.1 Ecovat storage tank

In the comparison of typical seasonal storage systems with buffer systems in section 2.3, it is stated that the size of storage tanks strongly depends on the available heat sources and requested heat demand. In setting up possible use cases, both, the capacity of the Ecovat storage tank as well as the amount of heat in- and output are free of choice. Therefore, it is chosen to fix the tank volume and expand the uses cases from this point forward. An Ecovat storage tank with a height of 32.4 [m] and diameter of 36.0 [m] is used for this use case, resulting in an h/d-ratio of 0.9 [-] and a volume capacity of 32,979 [m^3]. These dimensions are based on the volumes of buffer tanks included in section 2.2 and the available dimensions for Ecovat storage tanks (van den Bosch, 2019). Moreover, in section 1.1, it is introduced that the latest design of an Ecovat storage tank makes use of radial diffusers. For the chosen tank size, six diffusers are included in the tank, at which heights the tank can be charged and discharged, only.

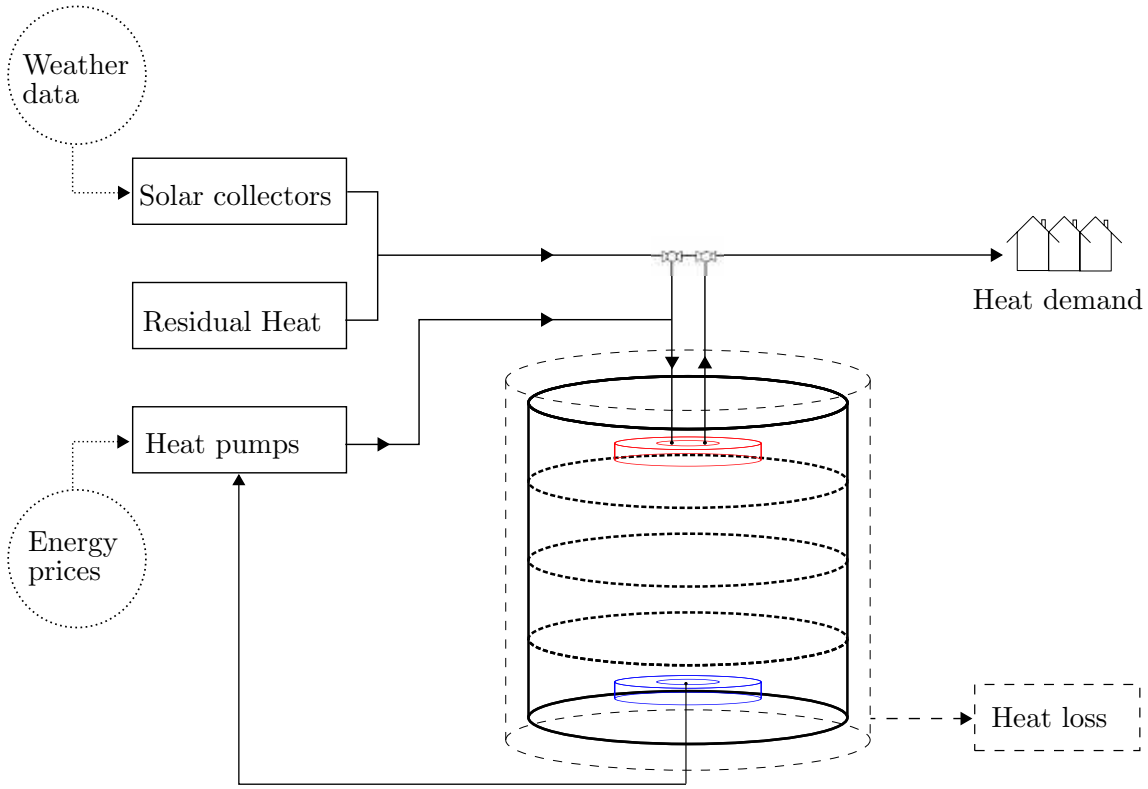

Figure 3.1: Schematics of the heat sources and demand included in the use cases. The heat sources of the use cases consist of solar collectors, residual heat from industry, and heat pumps. The total heat demand is based on the combined heat demand from a number of dwellings. Heat losses in the use cases are assumed to relate to the losses from the storage tank, only.

3.1.2 Heat demand

The future heat demand of a building is difficult to know without including a model of the building itself. Including this within the use cases is outside the scope of this study and makes a model unnecessary complicated. It is chosen, however, to base the heat demand on natural gas usage profiles. These profiles are obtained from Vereniging Nederlandse Energie Data Uitwisseling (NEDU), which is a data exchange platform for the Dutch energy industry, supervised by the government. The gas profile used for this study includes dwellings with a maximum annual natural gas usage of 5,000 [m^3]. The amount of gas used depends on the outside temperature, i.e. colder ambient temperatures naturally increase gas demand, when compared to warmer temperatures. This behaviour is also included within the profile and is translated to the following equation,

$$GP = \begin{cases} RER\,(T_{\text{heating}} - T_{\text{out}}) + TOP & \text{if } T_{\text{out}} < T_{\text{heating}}, \\ TOP & \text{if } T_{\text{out}} \geq T_{\text{heating}}, \end{cases} \tag{3.1}$$

where GP is the natural gas usage profile [-], RER a regression coefficient in [1/°C] describing the relationship between outside temperature and heating if necessary, TOP the temperature-independent part of the natural gas usage [-], T_{out} is the outside temperature based on the averaged temperature over the past years in [°C], and T_{heating} is the temperature from which

heating is necessary in [°C]. Summing the values for GP over a year results in 1.0 [-], representing the total natural gas usage of a dwelling (de Energiemanager, 2020).

Equation 3.1 relates to the fractions of natural gas demand over a year, only. In order to get the heating demand profile, a few additional steps have to be taken. First, the natural gas usage profile needs to be multiplied with the average gas demand, which is 1,340 [m^3] for dwellings in the Netherlands (Nibud, 2020). This average gas demand is based on all devices using natural gas; hence it also includes cooking. It is assumed that 5 [%] is used for cooking and the remaining 95 [%] for heating (Energievergelijken.nl, n.d.). Second, the natural gas demand should be multiplied with the calorific value of natural gas. This calorific value differs within a by law inserted range of values, which is based on different compositions of gas included in natural gas. However, for this study, it is assumed that the calorific value is constant and equals 35.09 [MJ/m^3](= 9.75 [kWh/m^3]) based on Dutch standards (van der Wal, 2003). The heat demand profile for one single dwelling, as presented in Figure 3.2 is obtained by combining the above-stated information.

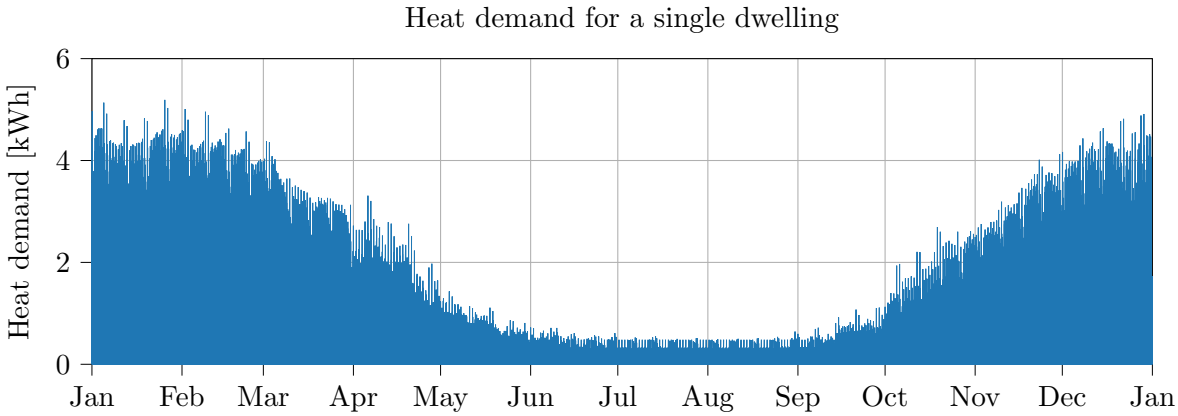

Figure 3.2: Heat demand for one single dwelling based on the average natural gas usage in 2019 within the Netherlands.

3.1.3 Heat sources

Similar heat sources as presented in chapter 2 are included in the use cases, consisting of heat pumps, solar collectors, and residual heat from the neighbouring industry. The use cases are designed in such a way that the heat from solar collectors and residual heat is supplied directly to the dwellings and only supplied to the storage tank when it overshoots heat demand. On the contrary, heat pumps provide to the storage tank only.

Heat pumps

Two types of heat pumps are included in the use case, air-water and water-water heat pumps. Air-water heat pumps (AWHPs) are heat pumps that compress ambient outside air to high-temperature air which is then exchanged to a water flow, increasing the water temperature that is supplied to the storage tank. Water-water heat pumps (WWHPs) operate by taking

water from the tank to the heat pump, which then helps to heat a stream of water which is pumped back into the hotter part of the storage tank. The operation of these heat pumps depend on their coefficient of performance (COP), maximum power, $P_{\mathrm{e,max}}$, and operation hours, $t_{\mathrm{operation}}$.

COP values of heat pumps are defined as the ratio of useful heating energy and the electric energy put in. This relation is put into the following equation,

$$\mathrm{COP} = \frac{Q_{\mathrm{useful}}}{P_{\mathrm{e}}}, \tag{3.2}$$

where Q_{useful} is the useful heating obtained from the heat pump in [$\mathrm{kW_{th}}$] and P_{e} is the inserted electric power in [$\mathrm{kW_e}$]. COP values are type depended, the types of heat pumps that are included in the use cases are based on the installed types at the Ecovat storage tank in Uden. Product specifications of these heat pumps give a range in which the COP differs as this is no constant value and depends on the in- and outgoing temperatures. However, in this study, COP values are assumed to be constant, which are validated in section 4.7. For the corresponding maximum power, a maximal number of heat pumps that are installed is set. The total capacities for the AWHPs and WWHPs are case-specific and are explained in section 3.2.

The heat pumps are included as a heat source to complement where the solar collectors and residual heat fall short. Their operation hours depend on two main factors, the amount of heat stored in the tank and the electricity price. First, the heat pumps must make sure enough heat is present in the storage tank to satisfy the heat demand, at all times, i.e. they should operate when a shortage of heat impends and not when the heat in the tank is sufficient to provide the heat demand. Second, the price of electricity determines whether the heat pumps are operating. The electricity price is not constant; however, it is depended on the supply and demand of electricity. This variation in price plays a significant role in charging and discharging behaviour of an Ecovat storage tank, i.e. it should be prevented that the heat pumps are operating when the electricity price is high but rather when it is low. In order to take these price variations into account, the so-called APX price is used within the designed use cases. The prices variations for 2019 are depicted in Figure 3.3 and are obtained from EDMij B.V., a company whose mission it is to supply validated energy data (Bartels, 2019).

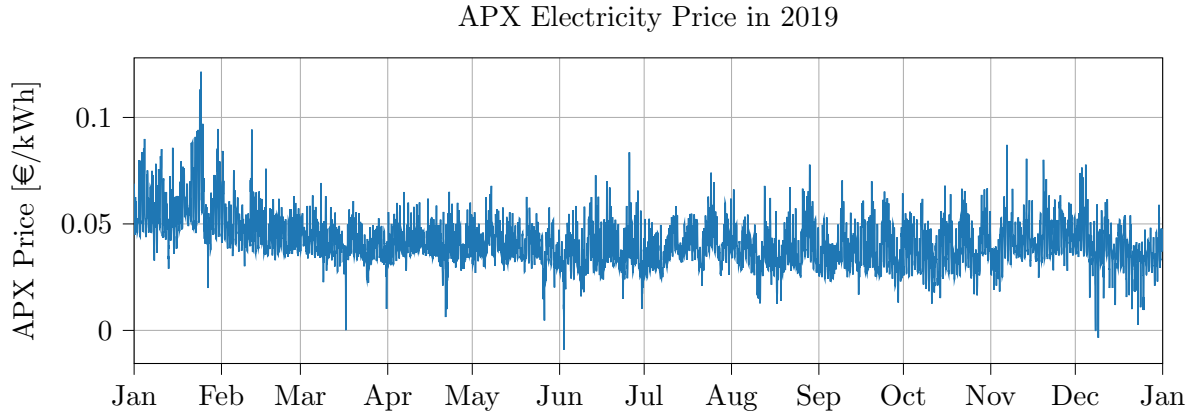

Figure 3.3: APX electricity prices for 2019 (Bartels, 2019).

Solar collectors

Solar collectors that are present within the designed use case supply energy directly to the dwellings. If there is energy left and thus overshoots the directly supplied heat demand, its energy is added into the Ecovat storage tank. The amount of solar energy is based on the efficiency of the collectors, total collector area, and the solar irradiation. This dependency is denoted as,

$$Q_{\text{solar}} = \eta_{\text{th}} G A_{\text{solar}}, \tag{3.3}$$

where Q_{solar} is the solar energy in [kWh], η_{th} the thermal efficiency of a single solar collector [-], G the solar irradiance in [kWh/m^2], and A_{solar} the combined solar area in [m^2].

The solar irradiance in Equation 3.3 is not constant throughout the year. Irradiance varies with time-of-day and during the year, i.e. no irradiance is present during the night, and for the summer months, more irradiance is present than winter months. The solar irradiance for the use cases is based on the irradiation profile measured in de Bilt, the Netherlands, in 2019, which is obtained from the Royal Netherlands Meteorological Institute (KNMI), the Dutch national weather service (KNMI, 2019). The irradiance profile is visualised in Figure 3.4.

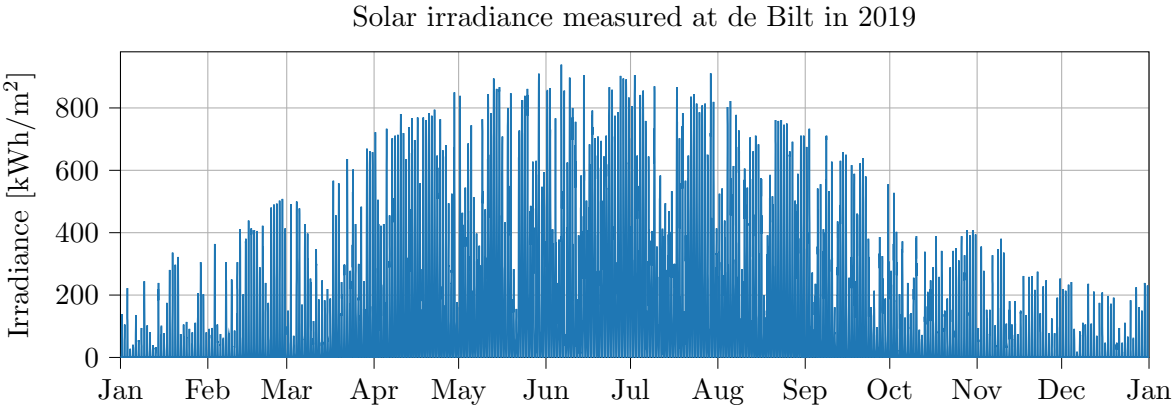

Figure 3.4: Solar irradiance as measured in 2019 at the weather station in de Bilt (KNMI, 2019).

Residual heat

In the use case, it is designed that there is sufficient neighbouring industry with residual heat available. This choice is based on the previously made overview of the already-in-place peak buffer storages, where most of them are located near industry, and the potential residual heat has to decrease CO_2 emissions significantly (Schepers & van Lieshout, 2011). The considered residual heat is thus treated as input heat for the tank. The available heat is assumed to be constant at all times during the year based on a continuously running industry.

3.2 Component Values

In subsections 3.1.1 - 3.1.3, the components included in the use cases are introduced. However, the amount by which a component is present for each of the use cases is not yet explained.

This section elaborates on the choices made regarding component values. These component values are used as input parameters for a model, which is presented in chapter 4.

The heat demand introduced in subsection 3.1.2 is for one single dwelling only. Therefore, to get the total heat demand, this profile is multiplied by a number of dwellings. In determining a suitable amount of dwellings for the seasonal use case, the maximum heat capacity for an Ecovat storage tank of 32,979 [m^3] is compared with the total annual heat demand of a single dwelling. The comparison shows that approximately 500 dwellings must be included to obtain a CN between 1.0 [-] and 2.0 [-]. In determining the number of dwellings for a buffer case, a different approach is used. Different sets of in- and output values are implemented within an Ecovat storage tank model. This information showed a range of feasible in- and output values for a peak buffer case and resulted in 2,500 dwellings.

With the total heat demand determined, a feasible set of input heat must be included in the use cases. At the Ecovat storage tank in Uden ≈ 0.15 [kW_{th}/m^3] is present to supply heat. In choosing the power of installed heat pumps for the seasonal use case, the order of magnitude of input heat of the Ecovat storage tank in Uden in combination with installed heat pumps within existing systems are kept in mind (Unsworth & Hoffmann, 2020). Taking this information into account, it results in a total electrical power of 1 [MW_e] for the seasonal use case. This total 1 [MW_e] is equally divided between the power of the AWHPs and the WWHPs, thus 500 [kW_e] of AWHPs and 500 [kW_e] of WWHPs. For the power of the peak buffer use case, it is chosen to linearly scale the power of the heat pumps and take an equal number of kilowatts per dwelling as is used for the seasonal use case.

The total surface of solar collectors expresses the amount of solar energy. In section 2.1, the total surface area covered by solar collectors in existing seasonal storage systems is discussed. In Friedrichshafen and Hanover ≈ 10 [m^2] solar collector per dwelling is present. Therefore, in this order of magnitude, solar collectors are also included in the seasonal use case. However, for these existing storage systems, there is no continuous presence of residual heat. Therefore, an area of 3 [m^2] per dwelling is used within the seasonal use case. For the peak buffer case, an Ecovat storage tank model showed that the same area of solar collectors per dwelling could result in too much input for the Ecovat storage tanks. Therefore, 1.5 [m^2] solar collectors per dwelling are chosen for the peak buffer case.

In section 2.2, the peak buffer storage systems are introduced. However, not much is stated about the amount of residual heat that is used within the storage systems. Therefore, it is chosen to take an amount of residual heat that covers the baseline of the heat demand, i.e. approximately the averaged summer demand. This demand is well below the found residual heat in Muller & Lensink (2020) and is therefore deemed to be a realistic amount for the use cases.

To conclude the use cases, an overview of these component values is given in Table 3.1.

Table 3.1: Overview of the component values for the use cases.

	Dwellings [-]	Residual heat [kW_{th}]	AWHP [kW_e]	WWHP [kW_e]	Solar collectors [m^2]
Seasonal case	500	150	500	500	1,500
Peak buffer case	2,500	225	2,500	2,500	3,750

3.3 Key Performance Indicators

Key Performance Indicators (KPIs) are defined to assess the use cases. It is essential to define representative and useful indicators to use in a comparison between the different use cases. If not, wrong conclusions might be obtained (Ochs, Heidemann & Müller-Steinhagen, 2009). The KPIs used in this study are the number of charging cycles, CN, the efficiency of the heat storage, η, equivalent CO_2 emissions, ε_{CO_2}, and the costs (Raab et al., 2005; Abdelhak et al., 2015; Dahash et al., 2019; Rijvers et al., 2020). In-depth descriptions of the stated KPIs are expressed below. Values for these KPIs are compared in chapter 5.

3.3.1 Number of charging cycles

The number of charging cycles [-], or cycle number (CN), states how often the maximum heat capacity of the Ecovat storage tank is discharged over a period of time. This is defined as the ratio of discharged heat and the maximum storage capacity, $Q_{\max}$, which is denoted as follows,

$$\mathrm{CN} = \frac{Q_{\mathrm{discharged}}}{Q_{\max}}, \tag{3.4}$$

with,

$$Q_{\max} = V_{\mathrm{tank}} \rho_{\mathrm{w}} c_{\mathrm{p,w}} \left(T_{\max} - T_{\min}\right), \tag{3.5}$$

where $Q_{\mathrm{discharged}}$ is the total discharged heat in [kWh], $Q_{\max}$ the maximum storage capacity in [kWh], V_{tank} the volume of the Ecovat storage tank in [m^3], ρ_{w} the density of water in [kg/m^3], $c_{\mathrm{p,w}}$ the specific heat capacity of water [kWh/(kg K)] and, $T_{\max}$ and $T_{\min}$ are, respectively, the maximum and minimum temperature in the tank in [°C] over a specified period of time.

To put the cycle number in context, an overview is added in Figure 3.5 presenting CN values for some of the storage systems included in chapter 2. However, it must be recognised that the CN is not always specifically mentioned in the literature, especially for the peak buffer systems. Therefore, some assumptions are made, which are explained in Appendix A. In Figure 3.5, on the left end of the line, the seasonal storage tanks are located, which generally have a CN of 1 - 2 [-]. On the other end, the day-to-night peak buffers are located for which the storage tank is completely charged and discharged daily, resulting in a CN of 365 [-]. In between these two extremes, storage tanks are classified. For example, the seasonal storage tank in Hanover has a CN that equals 1.5 [-] (Raab et al., 2005), the buffer tank in Theiß has a CN of $\approx$10 [-], and the buffer tank in Linz is discharged on a weekly basis, resulting in a CN of $\approx$50 [-] (Gimmelsberger, 2004).

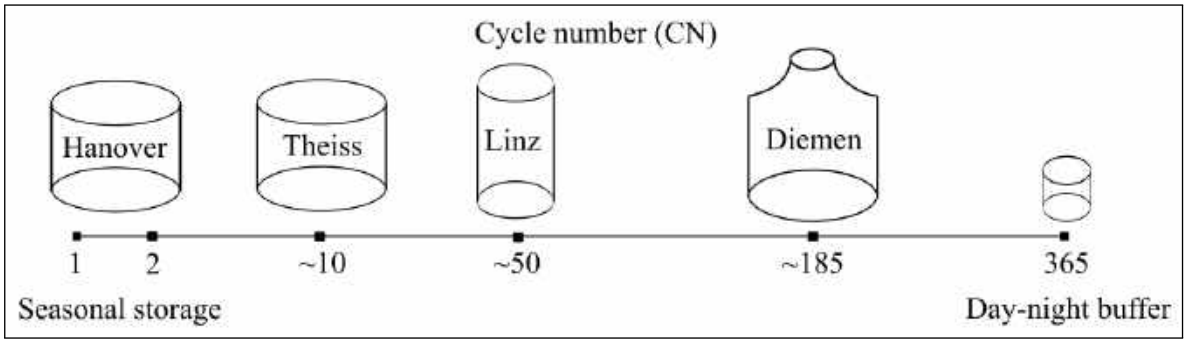

Figure 3.5: Representation of the number of charging cycles for various seasonal- and peak buffer systems. On the left end of the overview, the seasonal storage tanks are located, which generally have a CN of 1 - 2 [-]. On the other end, the day-to-night peak buffers are located for which the storage tank is completely charged and discharged daily, resulting in a CN of 365 [-].

3.3.2 Efficiency of the heat storage

The efficiency of the heat storage states how efficient the Ecovat storage tank stores heat over a specified period of time. This is defined as the ratio of useful heat that is discharged from the tank by heat charged into the tank, resulting in the following equation,

$$\eta = \frac{Q_{\text{discharged}}}{Q_{\text{charged}} - Q_{\text{diff}}} = 1 - \frac{Q_{\text{loss}}}{Q_{\text{charged}} - Q_{\text{diff}}}, \tag{3.6}$$

where Q_{charged} is the charged heat in [kWh], Q_{diff} is the difference in heat between the beginning and the end of a considered time period in [kWh], and Q_{loss} is the conductive heat loss of the Ecovat storage tank in [kWh].

3.3.3 Environmental performance indicators

Sustainability is one of the key purposes of Ecovat, and it is therefore important to also consider an environmental indicator, which is described by the 'equivalent CO_2 emissions' in [kton] (= 10^6 [kg]). These emissions are related to the electricity obtained from the grid to operate the heat pumps. In order to calculate the CO_2 equivalent emissions, use is made of the so-called CO_2 emission factor, which is a combination of the CO_2 emissions from the conversion and energy carriers that the power stations use. The factor expresses the equivalent CO_2 emissions, in [kg/kWh], for a specific electricity source. It is chosen to take the CO_2 emission factor of electricity for which the source is unknown, which equals 0.475 [kg/kWh] (SKAO, 2020). Combining the above information leads to,

$$\varepsilon_{CO_2} = 0.475 \int P_{\text{grid}} \, \mathrm{d}t, \tag{3.7}$$

where ε_{CO_2} is the equivalent CO_2 emissions in [kton] and $\mathrm{P_{grid}}$ is the electricity supplied by the grid in [$\mathrm{kW_e}$].

3.3.4 Costs

Ecovat wants to offer affordable heat to its customers; therefore, the costs are used as a performance indicator to compare use cases. The total costs of a system are divided into operational expenses (Opex) and capital expenditure (Capex), which is done for each of the system components of the use cases to get a clear overview of the costs.

Ecovat storage tank

The Capex of an Ecovat storage tank with a volume capacity of 32,979 [m^3] equals 226 [€/m^3], which results in a total of 7,458,000 [€]. The operational costs of the tank itself merely include maintenance costs, which are assumed to be 0.1 [%] of the Capex (van den Bosch, 2020).

Solar collectors

Solar collectors have an estimated Capex per square meter of 700 [€] based on a collector efficiency of 0.6 [-] (Lemmens, Beurskens & Lensink, 2020). The annual operational expenses of the solar collectors include maintenance costs, which are assumed to be 1 [%] of Capex (van den Bosch, 2020).

Residual heat

Residual heat is very case depended and heavily depends on the available heat at a given location. However, the Dutch Ministry of Economic Affairs and Climate ordered a market consultation performed by Muller & Lensink (2020) on residual heat in the Netherlands, which resulted in a price of 0.034 [€/kWh]. Note that no installation costs are assumed, and the residual heat is merely based on the consumed energy.

Heat pumps

The Capex for both, an AWHP and a WWHP is assumed to be equal to 430 [€/kW_e] (GEA, 2018), of which 200 [€/kW_e] is for the electrical necessities, i.e. transformers. The Opex of the heat pumps includes maintenance and electricity costs. The maintenance is assumed to be a constant value of 2 [%] and the electricity costs are based on the APX price and the annual electricity consumption, which is denoted as follows,

$$c_{\text{el}} = \int c\, P_{\text{grid}}\, \mathrm{d}t, \tag{3.8}$$

where c_{el} are the annual electricity costs in [€] and c is the APX price for electricity in [€/kWh], as presented in Figure 3.3.

Miscellaneous costs

In the realisation process of an Ecovat storage tank system, some costs cannot be determined in advance. Therefore, an estimated 5 [%] of the combined Capex is taken into account for unforeseen expenses (van den Bosch, 2020).

The Capex related costs, presented above, are made at the start when building an Ecovat storage tank. However, the period of interest in this study is a year. Therefore, the Capex is spread over the entire depreciation period of a system element, e.g. the depreciation period of the tank equals 50 years. This value, among others, for the system components their depreciation period are provided in Table 3.2 and 3.3.

Table 3.2: Costs of the components of the seasonal use case.

	Costs [€]	Period [yr]	Percentage [%]	Annual costs [€/yr]
Ecovat storage tank				
- Investment	7,458,000	50	-	149,160
- Maintenance	-	-	0.1	7,458
Solar Collectors				
- Investment	1,050,000	20	-	52,500
- Maintenance	-	-	1.0	10,500
Residual Heat				
- Operation	-	-	-	44,676
Heat pumps				
- Investment	430,000	20	-	21,500
- Maintenance	-	-	2.0	8,600
- Operation	-	-	-	TBD
Subtotal	8,938,000			
- Unforeseen	446,900	50	-	8,938
Total				303,332
Total per dwelling				606.67

Table 3.3: Costs of the components of the peak buffer use case.

	Costs [€]	Period [yr]	Percentage [%]	Annual costs [€/yr]
Ecovat storage tank				
- Investment	7,458,000	50	-	149,160
- Maintenance	-	-	0.1	7,458
Solar Collectors				
- Investment	2,625,000	20	-	131,250
- Maintenance	-	-	1.0	26,250
Residual Heat				
- Operation	-	-	-	67,014
Heat pumps				
- Investment	2,150,000	20	-	107,500
- Maintenance	-	-	2.0	43,000
- Operation	-	-	-	TBD
Subtotal	12,233,000			
- Unforeseen	611,650	50	-	12,233
Total				543,865
Total per dwelling				217.55

Chapter 4

Ecovat Storage System Model

To calculate the performance of the introduced use cases, explained in chapter 3, a model is to be developed. At first, the governing equations describing the Ecovat storage tank are introduced. These governing equations are followed by some assumptions and a short example. Next, the model is expanded by introducing optimisation, after which the corresponding equations are explained. To be certain, this developed model does represent a real-time Ecovat storage tank; it is validated in section 4.7. Following this, a convergence study for time and height is performed in section 4.8. To conclude, this chapter ends with known shortcomings and future improvements of the model.

4.1 Governing Equations

Fully mixed tanks are tanks with a homogeneous temperature distribution for which analytical solutions exist to determine the charging and discharging behaviour. However, in reality, temperature differences within a storage tank result in a difference in density, giving rise to buoyancy effects. These effects cause hotter water, with a lower density, to be located at the higher regions and the colder water, with a higher density, at the lower regions, resulting in a thermal stratification within the storage tank. For stratified tanks, analytical solutions cannot be presented. Therefore, in practice, numerical methods must be used (Zondag, 2019).

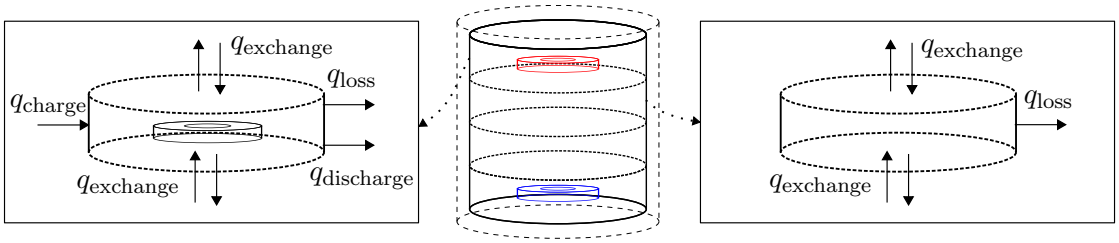

Figure 4.1: Schematics of the energy balance for the discretised layers. Left, a layer at which a diffuser is located is presented. Right, the remaining layers are presented.

To model the Ecovat storage tank, in which the degree of stratification is taken into account, the tank is discretised into several layers, N_{layers}. Each layer has a cylindrical shape as shown in Figure 4.1, and is treated as fully mixed with a homogeneous temperature distribution.

For each of the layers, conservation of mass, momentum, and energy hold. In addition, it is assumed that the mass of a layer is constant over time, no external forces apply, and water velocities are negligible, resulting that only conservation of energy is modelled. The system performs no work to its surroundings. Therefore, the change in energy is solely based on the addition or removal of heat, resulting in the following discretised energy balance for each layer,

$$\rho_{\mathrm{w},n} V_n c_{\mathrm{p},n} \frac{dT}{dt} = \sum_{i=1} q_{i,n} \qquad \forall\, n \in \{1, \ldots, N_{\mathrm{layers}}\}\,, \tag{4.1}$$

where V_n is the volume of layer n in [m^3], $c_{\mathrm{p,n}}$ the specific heat capacity of water of layer n in [kWh/(kg K)], and $q_{i,n}$ represents heat addition or removal term i on layer n in [$\mathrm{kW_{th}}$].

Worth mentioning is that these layers are not per se physically separated layers, i.e. there is no physical material separating the layers. It is a way to discretise the complete tank. By introducing these layers information gets lost, however. Suppose, a temperature distribution as shown in Figure 4.2(a) is present. Discretising and introducing layers to the model result in stepped temperature profiles as shown in Figure 4.2(b). This approximation of reality can be improved by increasing the number of layers within the model. The disadvantage of this being the increase in computation time. The number of layers used while solving the use cases is based on the convergence study as presented in section 4.8.

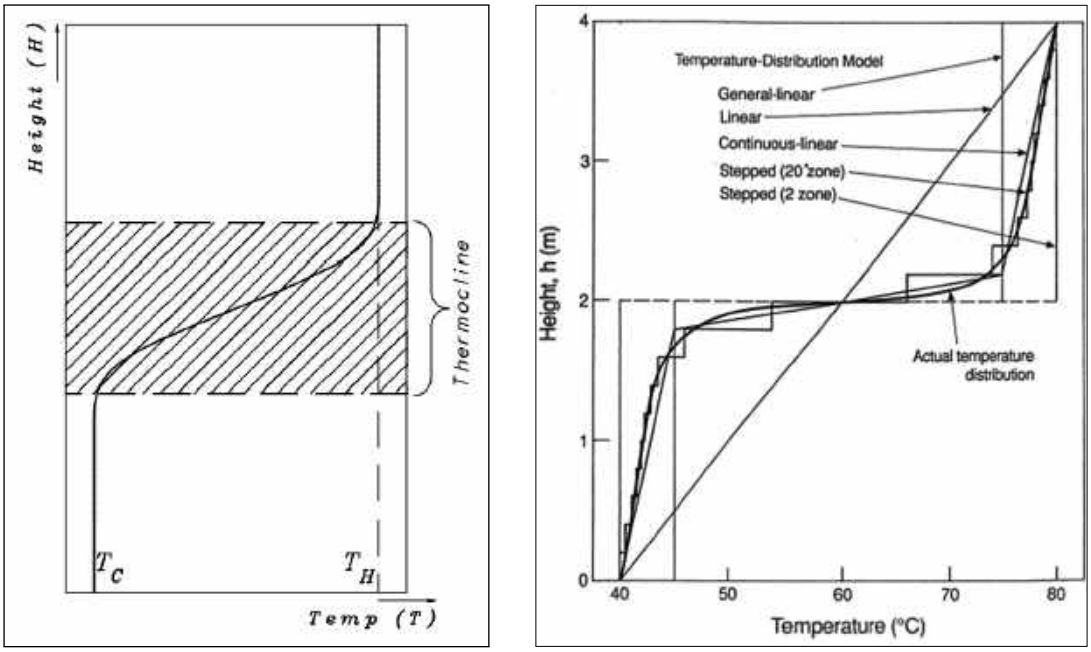

(a) (b)

Figure 4.2: (a) Realistic temperature distribution within a storage tank. A thermocline is present in a stratified tank and is located between layers where an abrupt temperature gradient occurs. (b) Discretising this temperature distribution introduces a loss in information (Njoku et al., 2014).

To solve the energy balance, the time horizon is discretised into a number of time intervals. Introducing a Forward Euler discretisation scheme in Equation 4.1 results for layer n at time t, the following equation,

$$\rho_{\mathrm{w},n} V_n c_{\mathrm{p},n} \frac{T_n(t) - T_n(t-1)}{\Delta t} = \sum_{i=1} q_{i,\,n,\,t-1} \quad \forall\, n \in \{1, \ldots, N_{\mathrm{layers}}\}\,,\; t \in \{1, 2, \ldots, N_{\mathrm{time}} + 1\}\,, \tag{4.2}$$

where T_n is the temperature of layer n in [°C] and Δt is the time step in [hr].

Rewriting Equation 4.2 and substituting heat addition or removal terms, results in a discretised temperature change as presented below,

$$T_n(t) = T_n(t-1) + \frac{1}{\rho_{\mathrm{w},n} V_n c_{\mathrm{p},n}} \left(q_{\mathrm{charge},\,n,\,t-1} - q_{\mathrm{discharge},\,n,\,t-1} + q_{\mathrm{exchange},\,n,\,t-1} - q_{\mathrm{loss},\,n,\,t-1}\right) \Delta t, \tag{4.3}$$

where $q_{\mathrm{charge},\,n,\,t-1}$ is the heat charged to layer n at time $t-1$ in [$\mathrm{kW_{th}}$], $q_{\mathrm{discharge},\,n,\,t-1}$ is the heat discharged from layer n at time $t-1$ in [$\mathrm{kW_{th}}$], $q_{\mathrm{exchange},\,n,\,t-1}$ is the conductive heat exchanged with surrounding layers to n at time $t-1$ in [$\mathrm{kW_{th}}$], and $q_{\mathrm{loss},\,n,\,t-1}$ is the conductive heat loss to the surroundings from layer n at time $t-1$ in [$\mathrm{kW_{th}}$].

In Equation 4.3, the heat addition and removal terms are divided into four components, charging, discharging, conductive heat transfer between layers and conductive heat losses to the surroundings. The charging and discharging term relate to the layers in which diffusers are present, only, and equal zero for the remainder, as visualised in Figure 4.1. Each of the heat exchanging components is explained in more detail below. For convenience, from here on, n is removed as subscript if it is non-essential for an equation.

Charging terms

The charging term, q_{charge}, is defined as,

$$q_{\mathrm{charge}} = q_{\mathrm{solar}} + q_{\mathrm{WWHP,\,h}} + q_{\mathrm{AWHP}} + q_{\mathrm{residual}}, \tag{4.4}$$

where q_{solar} is the heat obtained from solar collectors based on Equation 3.3, $q_{\mathrm{WWHP,\,h}}$ and q_{AWHP} represent the heat charged by the heat pumps and q_{residual} is the residual heat in [$\mathrm{kW_{th}}$]. The heat that is charged by the heat pumps is defined as,

$$q_{\mathrm{WWHP,\,h}} = \mathrm{COP}_{\mathrm{WWHP}} \cdot P_{\mathrm{e,\,WWHP}}, \tag{4.5}$$

$$q_{\mathrm{AWHP}} = \mathrm{COP}_{\mathrm{AWHP}} \cdot P_{\mathrm{e,\,AWHP}}, \tag{4.6}$$

where COP is the coefficient of performance [-] and P_{e} the electrical power driving the heat pumps in [$\mathrm{kW_e}$].

Discharging terms

The discharging term is represented by the follow equation,

$$q_{\mathrm{discharge}} = q_{\mathrm{WWHP,\,c}} + q_{\mathrm{demand}}, \tag{4.7}$$

where q_{demand} is the heat demand supplied to the dwellings in [kW_{th}] and $q_{\text{WWHP, c}}$ is the heat that is supplied into the cold side of the WWHPs to increase the temperature of the water at the warm side, which is defined as,

$$q_{\text{WWHP, c}} = (\text{COP} - 1)P_{\text{e, WWHP}}. \tag{4.8}$$

Conduction terms

The heat loss from the tank to its surroundings, q_{loss}, and conduction between water layers, q_{exchange}, are given by the following equations,

$$q_{\text{loss}, n, t-1} = UA_{\text{side}}(T_n(t-1) - T_{\text{ground}}), \tag{4.9}$$

$$q_{\text{exchange}, n, t-1} = \frac{\kappa_{\text{w}}}{\Delta h}\frac{\pi}{4}d^2\,(T_{n+1}(t-1) + T_{n-1}(t-1) - 2T_n(t-1)), \tag{4.10}$$

where U is the overall heat transfer coefficient in [$\text{W}/(\text{m}^2\text{K})$], A_{side} the area separating a layer and the surroundings in [m^2], T_{ground} the ground temperature in [°C], κ the conductive heat transfer coefficient of water [W/(m K)], d the diameter of the Ecovat storage tank, and Δh the height of a discretised layer, both in [m].

4.2 Assumptions

Modelling complex physical phenomena, in general, requires additional assumptions in order to simplify the considered problem. In doing so, one effectively decreases the model complexity and computational effort. Therefore, making well-founded assumptions is important. In this section, the assumptions that are applied in the model are pointed out. These assumptions are divided into two subsections, one for the assumptions related to the tank itself and one to the remaining system components.

4.2.1 Ecovat storage tank

Several assumptions are made regarding the storage tank itself.

Dimensions of the storage tank

This assumption is indirectly already introduced within the discretisation but not yet specifically mentioned. It is assumed that there is only temperature variation in different layers distributed along with the height of the tank, reducing the model to a one-dimensional problem. The dimensions of the layers are based on a perfect cylinder, which in reality not the case as the tank exists out of pre-fabricated concrete wall parts, which are not entirely smooth and are placed in such a way that the tank approaches a circle.

Constant insulation

The insulation thickness is not distributed uniformly in reality. More specifically, the insulation is minimal at the bottom of the tank, as the lowest temperature and therefore heat losses are present here. This non-uniformly distributed insulation reduces the usage of insulation materials, hence reduces the costs of the tank. In the model, however, it is assumed that walls and the floor have the same level of insulation. It is chosen to take overall heat transfer coefficients as obtained in the validation, section 4.7.

Water properties

Water properties such as the specific heat, $c_{p,w}$, density, ρ_w, and thermal conductivity, k, are taken as constants, which is preferred over taking these values as variables. The reduction of the need for computationally heavy operations is expected to be more important than the improvements of variable water properties would have on the final results. By setting these properties constant, minor uncertainties are introduced. The density of water is set to ρ_w = 981 [kg/m^3], the specific heat value to $c_{p,w}$ = 0.00165 [kWh/(kg K)], and the thermal conductivity to k = 0.635 [W/(m K)]. These properties are based on an averaged value for a temperature range of 5 - 95 [°C], resulting in a maximal deviation for the density, specific heat, and thermal conductivity of, respectively, ± 2 [%], ± 0.3 [%], and ± 6 [%].

No leakage

It is assumed that the tank does not leak, although this not the case for the test site, in Uden two types of leakages occur. First, there is a thermal leak in between two layers of pre-fab concrete walls. During construction, the alignment of these layers was faulty and had to be filled up with extra concrete instead of insulation material. Second, water can leak out of the Ecovat storage tank at the bottom as this is not entirely watertight. For future Ecovat storage tanks, these errors are not expected nor allowed and are therefore not accounted for in the model of this study.

Ground temperature

The temperature of the ground surrounding the Ecovat is taken constantly at 10 [°C]. In reality, this temperature is not constant as the warm temperatures within the tank increase the temperature of the surrounding ground. This effect is however set to be negligible to the considered period of interest of maximum a year compared to the time it takes to heat the surrounding ground to be of influence on the tank. Note that this increase in ground temperature is eventually profitable for the performance of underground storage tanks as the temperature difference between the inside of the tank and its surrounding decreases. Hence, the losses from the tank to the ground decreases.

4.2.2 Further system components

In section 3.1, all systems components are already described. Hence, some assumptions are previously mentioned; nevertheless, these are included in this section to create a complete overview.

Efficiency solar collectors

The efficiency of solar collectors is set to be a constant value of 0.6 [-]. In reality, this is not the case. Namely, the efficiency of solar collectors depends on multiple factors like the in- and outgoing temperatures and ambient temperatures. However, implementing these factors is outside the scope of this study.

Piping losses

The heat losses in the model are merely based on the conductive heat losses from the storage tank. It is assumed that the piping is ideally insulated such that no heat is lost. In reality, this is not the case as pipes are only insulated to a certain extent and heat is lost. These piping losses are depended on the temperature and total piping length, modelling this is outside the scope of this study, however.

Full load hours residual heat

The residual heat obtained from neighbouring industry is assumed to be equal at all times during the year, representing a continuously running industry. This continuously running industry is not entirely realistic. In reality, it depends heavily on the working hours and intensity of the industry. However, taking the working hours and intensity requires additional research, which is not the main focus of this study. For this study, the constant supply of residual heat is deemed to be sufficient. It is acknowledged, that a more realistic residual heat profile might help to make a more representative case and real-life representation for the optimisation. Therefore, it is recommended to conduct additional research on these profiles in the future.

Temperature residual heat

It is assumed that the temperature obtained from residual heat is high, and therefore no additional heating has to be performed by heat pumps. In reality, several industries are present for which this assumption holds (Muller & Lensink, 2020). However, it is noted that this assumption does not hold for every residual heat source. If the temperature is not high enough, heat pumps are necessary to upgrade these temperatures, which then needs to be modelled as well.

Heat pumps COP values

The COP values of the heat pumps are assumed to be constant and equal to 2.4 [-] and 3.0 [-] for the AWHP and WWHP, respectively. These are based on the product specifications and charging validation presented in subsection 4.7.2.

4.3 Example

In this section, an example is given visualising the in- and output of the Ecovat storage tank model. The dimensions of the modelled tank are based on the Ecovat storage tank in Uden, which has a height of 13.9 [m] and diameter of 10.9 [m], resulting in a volume of 1,302 [m^3]. The tank is discretised into four layers, in which heat can be charged and discharged.

In this example, the first week of April is simulated. The total heat demand that is discharged from the tank is based on 185 dwellings, which results in a discharging profile, as presented in Figure 4.3(a). The heat from the solar collectors and residual heat is used to charge the tank as presented in Figure 4.3(b). These sources are based on 200 [m^2] solar collectors combined with the solar irradiance profile for the first week of April and a constant residual heat of 50 [kW_{th}]. The charging profile is then obtained by subtracting the directly supplied heat to the dwellings from the sources. Besides, heat pumps are used to charge the storage tank. In this example, merely heat from WWHPs are included; thus, no AWHPs are present. The electric power profile of the WWHPs is presented in Figure 4.3(c). For this charging profile, it is assumed that the heat pumps operate continuously for 6 hours every 12 hours.

Solving for these charging and discharging profiles with a time step of 15 [min] results in a temperature profile as presented in Figure 4.3(d). The electricity costs for this week equal 94.57 [€] and the equivalent CO_2 emissions 997.5 [kg]. These performance indicators, as introduced in section 3.3, are based on the operation of the heat pumps. The charging profile for this example is given as predetermined input for the model. However, it might be possible that the heat pumps operate too much or at times the electricity price is at a high value. This predetermined charging profile thus results in higher electricity costs and equivalent CO_2 emissions than necessary, therefore underperforming compared to what might be possible.

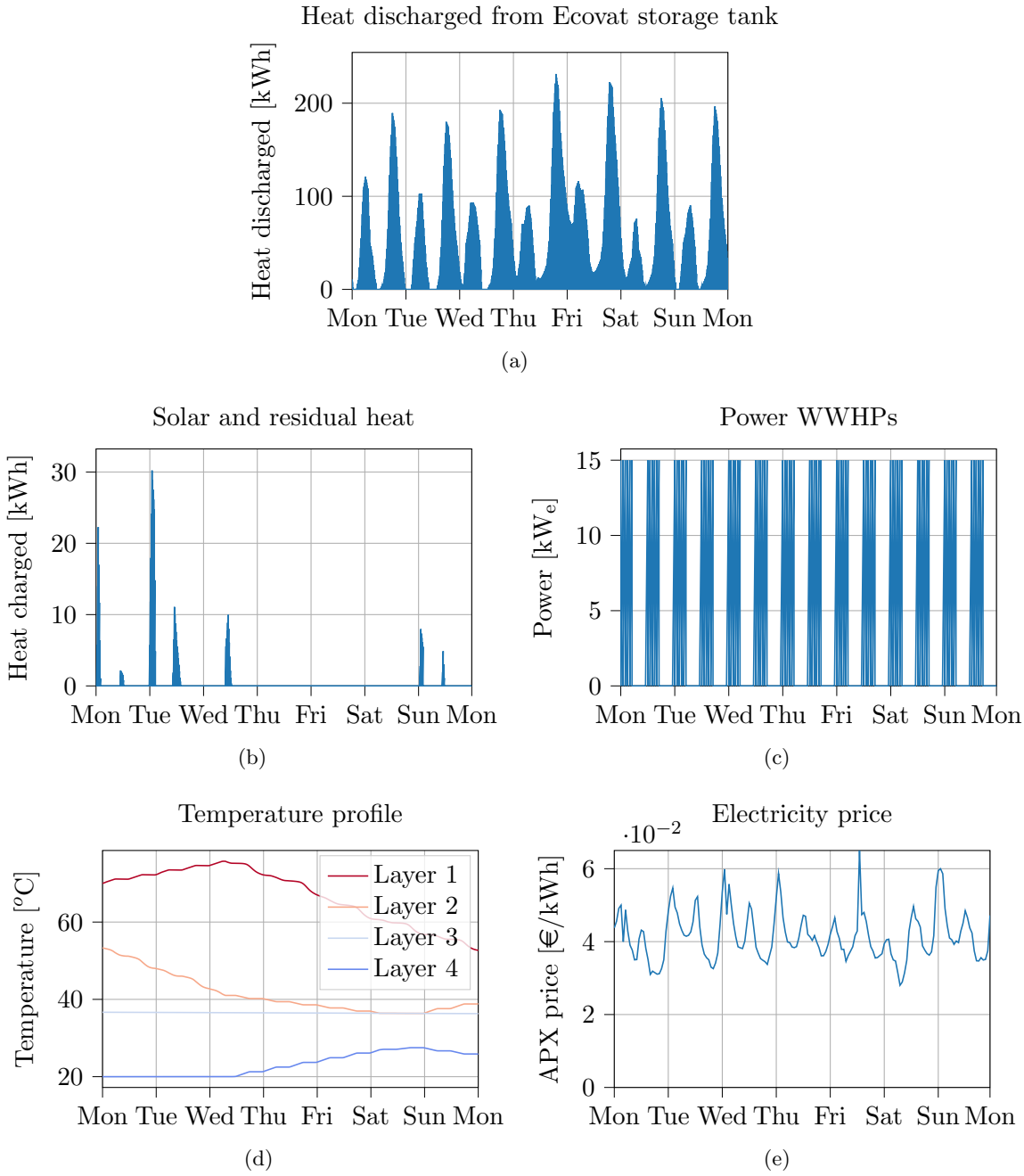

Figure 4.3: (a) Heat discharged from the Ecovat storage tank. (b) Heat charged to the Ecovat storage tank, supplied by the solar collector and residual heat. (c) Electric power profile to operate the WWHPs. (d) Temperature profile for the simulated example. (e) APX electricity price for the first week of April.

4.4 Convex Optimisation

In section 4.3, an example of the Ecovat storage tank is presented, where it is stated that predetermined charging profiles might lead to underperformance of the Ecovat storage tank. Therefore, to compare the use cases, as introduced in chapter 3, it is important that the charging and discharging strategies are optimal. If this would not be the case, it might well be possible that an optimal profile is compared with a non-optimal profile. Comparing the performance of an Ecovat storage tank while it is performing as desired with an underperforming case, gives a non-reliable comparison reducing the quality of the analysis. To get an optimal charging and discharging profile, the use cases are modelled using an optimisation model, more specifically, a convex optimisation model. This type of optimisation is chosen because of various reasons. At first, it is stated that general optimisation problems are difficult to solve and generally include some compromise, such as very long computation times, or the possibility of not finding the solution. However, if a problem is formulated as a convex optimisation problem, it can be solved efficiently (Boyd & Vandenberghe, 2004). Secondly, a fundamental statement of convex optimisation holds that 'a local optimum is a global optimum' (Ledyard & Chandy, 2005). Finally, within the research team of Ecovat, a proof-of-concept has been developed in the past, showing the potential of a convex optimisation model (de Ridder & Mazairac, 2019).

A convex optimisation problem is of the form,

$$\begin{aligned} &\text{minimise} \quad f(\boldsymbol{x}), \\ &\text{subject to} \quad \boldsymbol{g}(\boldsymbol{x}) \geq \boldsymbol{b}, \end{aligned} \tag{4.11}$$

where $f(\boldsymbol{x})$ is the objective function which has to be minimised, $\boldsymbol{x}$ is a vector containing the optimisation variables, also referred to as decision variables, $\boldsymbol{g}(\boldsymbol{x})$ is the vector which holds the governing equations and constraints of the problem, and $\boldsymbol{b}$ holds the budget values. The objective function is explained in more detail in section 4.5 and the governing equations and constraints in section 4.6.

This convex optimisation model is coded in Python 3.7 and makes use of the CVXPY module. CVXPY is a python embedded modelling language for convex optimisation problems (Diamond & Boyd, 2016).

4.5 Objective Function

The objective function, $f(\boldsymbol{x})$, states what variable(s) are optimised e.g. the heat losses or equivalent CO_2 emissions are possible variables that can be optimised for the system. However, the total costs of a system are important in deciding if sustainable technologies are implemented or not. If the costs of technology become too high, it increases the overall costs of the energy transition and loses general support (Stratelligence, 2020). Combining this with Ecovat's aim to supply affordable heat to its customers, the annual costs are set to be optimised. The total annual costs are described in subsection 3.3.4 consisting of Capex and Opex. The Capex is case-specific and is not optimised. The Opex includes annual maintenance costs, which are assumed to be a constant percentage each year, and the electricity costs to operate the heat pumps. Therefore, the electricity costs of the heat pumps are optimised, resulting in the following objective function,

$$f(P_{\text{grid}}) = \int c\, P_{\text{grid}}\, \mathrm{d}t, \tag{4.12}$$

where c are the costs of electricity at a certain moment in time in [€/kWh] presented in Figure 3.3 and $\mathrm{P_{grid}}$ is the electricity supplied by the grid in [$\mathrm{kW_e}$].

ADMM algorithm

As Equation 4.12 is an affine function, proven in section B.1, it can be solved using convex optimisation. Solving convex optimisation problems cannot be done analytically (Boyd & Vandenberghe, 2004). Nevertheless, there are effective methods for solving them. The model used in this study is solved by means of the alternating direction method of multipliers (ADMM). ADMM is an algorithm that solves convex optimisation problems by breaking the problem in multiple smaller problems, making it a fast way to solve the general problem. The derivation towards an ADMM compatible objective function is presented in section B.2. Equation 4.12 is updated and becomes as follows,

$$\begin{aligned} f(P_{\text{grid}}, T_m, \lambda_{\text{init}}, \lambda_{\text{term}}) = \int & c\, P_{\text{grid}}\, \mathrm{d}t \\ & + \phi_{\text{init}} \left(\lambda_{\text{init}} \left(T_{m,0} - \overline{T}_{\text{init}} \right) + \frac{1}{2} \alpha \left(T_{m,0} - \overline{T}_{\text{init}} \right)^2 \right) \\ & + \phi_{\text{term}} \left(\lambda_{\text{term}} \left(T_{m,\text{end}} - \overline{T}_{\text{term}} \right) + \frac{1}{2} \alpha \left(T_{m,\text{end}} - \overline{T}_{\text{term}} \right)^2 \right), \end{aligned} \tag{4.13}$$

where T_m is the temperature distribution during period m in [°C], $T_{m,0}$ and $T_{m,\text{end}}$ include the initial and terminal temperature per layer of the period m, respectively, $\overline{T}_{\text{init}}$ is the average temperature of a layer between the initial temperature of period m and the terminal temperature of period m - 1, $\overline{T}_{\text{term}}$ is the average temperature of a layer between the terminal temperature of period m and the initial temperature of period m + 1, ϕ_{init} is a state parameter which equals 0 when $m = 0$ and equals 1 for the remaining periods, ϕ_{term} is a state parameter which equals 0 when the final period is optimised and equals 1 for the remaining, α is a non-dimensional parameter that helps the ADDM algorithm converge, the so-called penalty parameter, λ_{init} and λ_{term} are Lagrangian multipliers that help periods match temperatures to the other periods.

The introduction of the ADMM algorithm thus splits the total period of interest, i.e. a year, into m different periods. Due to this splitting, initial and terminal temperatures of periods are matched to represent the charging and discharging behaviour for a year. This matching of different periods is visualised in Figure 4.4.

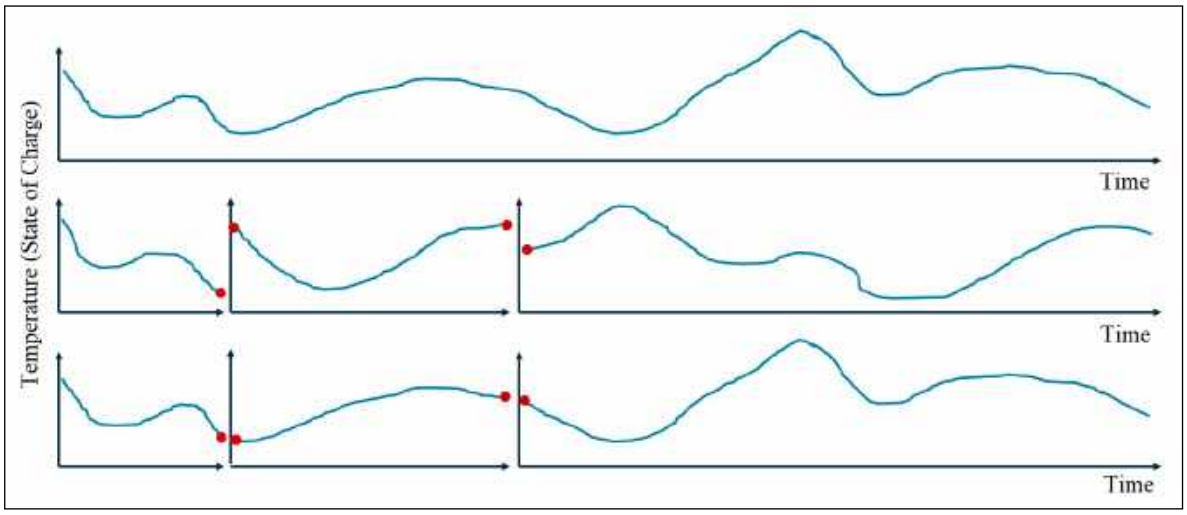

Figure 4.4: The temperature at the beginning of a period should match the temperature at the end of the previous period (de Ridder & Mazairac, 2019).

Temperature distribution penalty

In the optimising process, the most suitable height at which heat is exchanged is determined. In doing so, a penalty value is assigned to the objective function when an unrealistic temperature distributions is present within the tank. Suppose, a high amount of heat is suddenly injected into the coldest layer at the bottom of the tank. The temperature of this bottom layer becomes higher than the layer above it, which is physically unrealistic. This unrealistic temperature distribution then results in a penalty with a factor 10^5 added to the objective function, which thus increases greatly. The addition of the penalty value finalises the objective function from Equation 4.13 to,

$$\begin{aligned} f(P_{\text{grid}}, T_m, \lambda_{\text{init}}, \lambda_{\text{term}}) = \int & c\, P_{\text{grid}}\, \mathrm{d}t + 10^5\, \delta\, T_m \\ & + \phi_{\text{init}} \left(\lambda_{\text{init}} \left(T_{m,0} - \overline{T}_{\text{init}} \right) + \frac{1}{2} \alpha \left(T_{m,0} - \overline{T}_{\text{init}} \right)^2 \right) \\ & + \phi_{\text{term}} \left(\lambda_{\text{term}} \left(T_{m,\text{end}} - \overline{T}_{\text{term}} \right) + \frac{1}{2} \alpha \left(T_{m,\text{end}} - \overline{T}_{\text{term}} \right)^2 \right), \end{aligned} \tag{4.14}$$

where δ is an auxiliary multiplier which equals 1 if the temperature distribution is unrealistic and 0 if this is not the case.

Nevertheless, if an unrealistic temperature is obtained, the model mixes involved layers until a realistic temperature distribution is again obtained. The layers are mixed until the objective function is no longer penalised. In reality, this mixing of layers correlates to convection.

However, in section 4.1, it is mentioned that the velocity field is assumed to be zero and convection terms are not taken into account, as these terms make the model more complex and computational heavier than desired. Therefore, this mixing of layers is simplified by averaging the temperatures of layers (Lago et al., 2019). To visualise this mixing effect, an initial temperature distribution, as presented in Figure 4.5(a), is inserted in the model after which it mixes the layers around until the penalty value is no longer assigned to the objective function. The model results a temperature profile as presented in Figure 4.5(b). It is observed that the overall temperature in the tank is completely averaged after a matter of hours.

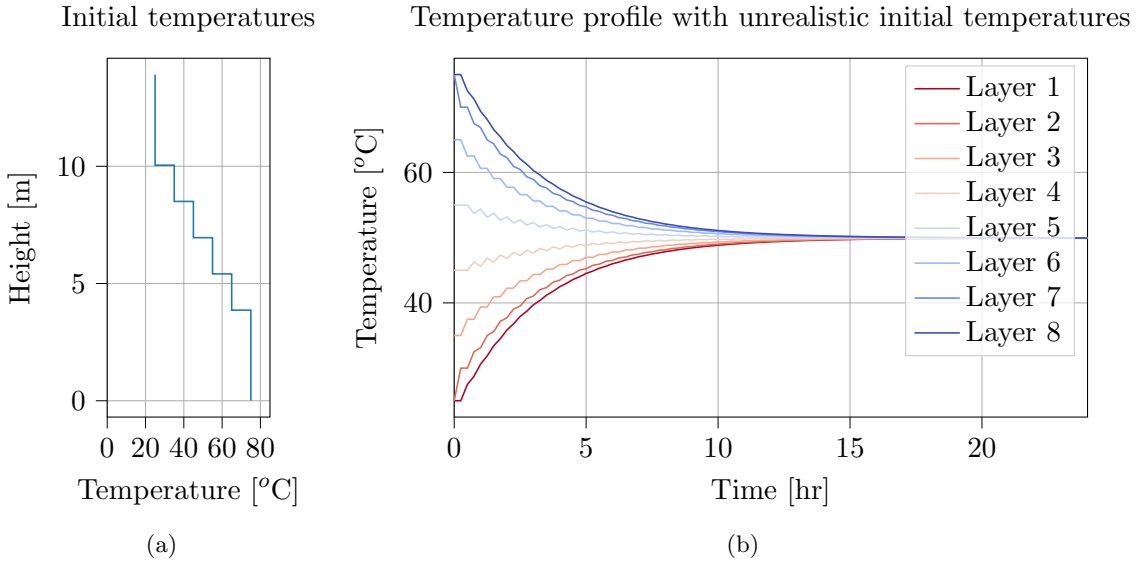

Figure 4.5: (a) Unrealistic initial temperature distribution. (b) Temperature profile showing the mixing of layers when an unrealistic initial temperature profile is inserted into the model.

Discretisation

To model the objective function, it has to be discretised in time and for the number of layers. Therefore, Equation 4.14 for period m is discretised and is denoted as follows,

$$
\begin{aligned}
f_m(P_{\text{grid}}, T_m, \lambda_{\text{init}}, \lambda_{\text{term}}) = \sum_{n=1}^{N_{\text{layers}}} \Bigg(& \sum_{i=1}^{N_{\text{time}}} \left(c_i \, P_{\text{grid},n,i} \, \Delta t + 10^5 \, \delta \, T_{m,n,(i-1)} \right) \\
& + \phi_{\text{init}} \left(\lambda_{\text{init}} \left(T_{m,n,0} - \overline{T}_{n,\text{init}} \right) + \frac{1}{2} \alpha \left(T_{m,n,0} - \overline{T}_{n,\text{init}} \right)^2 \right) \\
& + \phi_{\text{term}} \left(\lambda_{\text{term}} \left(T_{m,n,\text{end}} - \overline{T}_{n,\text{term}} \right) + \frac{1}{2} \alpha \left(T_{m,n,\text{end}} - \overline{T}_{n,\text{term}} \right)^2 \right) \Bigg).
\end{aligned}
\tag{4.15}
$$

4.6 Constraints

The objective function is subjected to a set of governing equations and constraints, as mentioned in section 4.4. The governing equations included in the model are presented in section 4.1. Additionally, constraints apply to the convex optimisation problem and are denoted as follows:

- The six diffusers that are present in the tank are equally spaced over the height of the tank. Limiting the heights at which heat can be charged and discharged from the tank to six fixed positions;
- Heat that flows into the cold side of the WWHPs, $q_{\mathrm{WWHP,\,c}}$, can only be discharged from the bottom three diffusers;
- The discretised layers may not exceed a maximum temperature, $\mathrm{T_{top}} \leq T_{\mathrm{limit,top}}$. This boundary condition is induced because the pressure is not included into the model, but it should satisfy the thermodynamic laws where water at atmospheric pressure starts boiling at $\approx$100 [°C]. Therefore, a maximum temperature of 98 [°C] is included, preventing water in the storage tank from boiling;
- The top six layers may not drop below their minimal temperature limit of 57 [°C], $\mathrm{T_{top}} \geq T_{\mathrm{limit}}$. These upper layers must stay above a temperature limit to make sure the tank is not discharged too much, a temperature of 57 [°C] is chosen as this is just above the common supply temperature to the district heating network (Niessink, 2020);
- The discretised layers may not exceed a minimum temperature of 10 [°C], $\mathrm{T_{bottom}} \geq T_{\mathrm{limit,bottom}}$. This boundary condition is induced to make sure that the water stays away from the freezing point. The limiting temperature is based on the ground temperature.
- To keep stratification and keep the mixing to a minimum, a constraint is included restraining the maximum heat exchanged at the radial diffusers during a time step Δt. Therefore, the exchanged heat must be lower than the maximum heat exchange of the diffusers based on a maximum flow rate of 500 [m^3/hr] and temperature difference of 30 [°C]. A temperature difference of 30 [°C] is used as this is common for district heating systems (Niessink, 2020). Ideally, this should be determined with the actual temperatures. However, this relates to the circulation zones which are not yet implemented, explained in more detail in section 4.9.
- The power of the heat pump is specified within an operating range, $0 \leq P_{\mathrm{HP}} \leq P_{\mathrm{HP,\,max}}$.

4.7 Validation

The model is validated using the data obtained from the Ecovat storage tank in Uden. In Figure 4.6, a cross-section of this tank is presented. This Ecovat storage tank is used to validate the model. The validation is done based on two scenarios, one for the heat loss over time without any charging or discharging performed and one for the charging process. Furthermore, the objective function and optimisation algorithm are validated in sections B.3 and B.4, respectively.

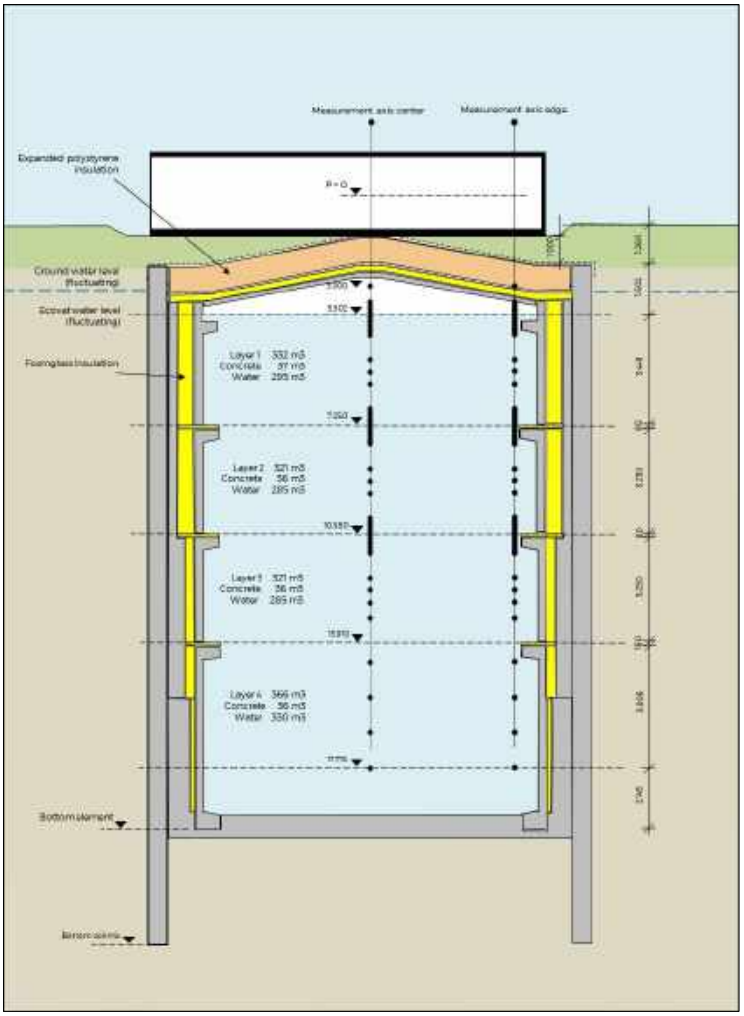

Figure 4.6: Schematic cross-section of the Ecovat storage tank in Uden. In this figure, the black dots are temperature sensors that are installed within the tank. Moreover, the yellow coloured part is foam glass insulation, the orange coloured part is expanded polystyrene (EPS), and the grey coloured part is concrete.

4.7.1 Heat loss over time

An experiment was performed in the past to prove the efficiency of the Ecovat as a storage tank. During this experiment, the tank is charged until 6^{th} of September 2017. After this date, for 26 consecutive weeks, the temperature is measured weekly at several depths on two axes along the vertical direction, one near the wall and one in the centre of the tank. During this period of 26 weeks, no heat added or extracted.

The temperatures obtained during the 26 weeks are translated to four uniform temperatures, one for each considered discretised layer. This translating is firstly done by merging the measurements from two vertical axes into one temperature per depth. After this merging, temperatures are corrected for the difference in water level and combined into averaged temperatures for the layers. Correcting for the fluctuations in water level helps to increase the

certainty of measured data. As mentioned in subsection 4.2.1, due to construction failures, the bottom of Ecovat storage tank in Uden is not watertight, allowing the water level to vary. Therefore, during the weekly temperature measurements, the water level was measured as well, which results in the water level profile, as presented in Figure 4.7.

Taking the steps as mentioned above, a heat loss temperature profile as presented by the blue lines in Figure 4.8 is obtained. An uncertainty of 0.1 [°C] is included in the measured data. This uncertainty is solely based on the test certificate of the MH 3710 temperature sensors (SIKA, n.d.).

From a previously conducted internal research, the thermal resistances were calculated (van den Bosch, 2018). These are used for the validation of the heat loss, resulting in thermal resistances of $R_{wall} = 5.25$ [m^2 K/W] and $R_{top} = 4.05$ [m^2 K/W]. With these thermal resistances, a temperature profile as presented with the red lines in Figure 4.8 is obtained. It is observed that the model follows the measured data well. Therefore, it is stated that the heat losses included in the model are representative of the Ecovat storage tank in Uden.

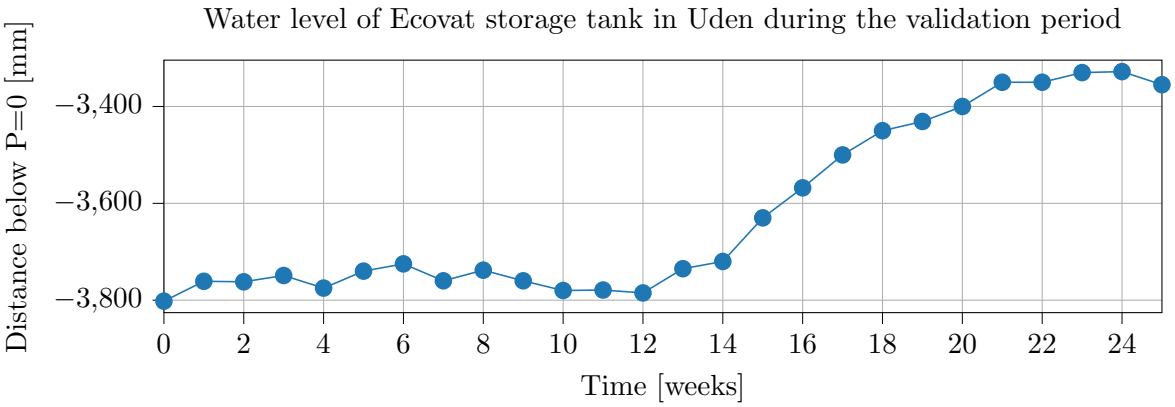

Figure 4.7: Measured water level of the Ecovat storage tank in Uden during the validation period of the heat loss. The water level is measured from P = 0, shown in Figure 4.6, to the top of the water level.

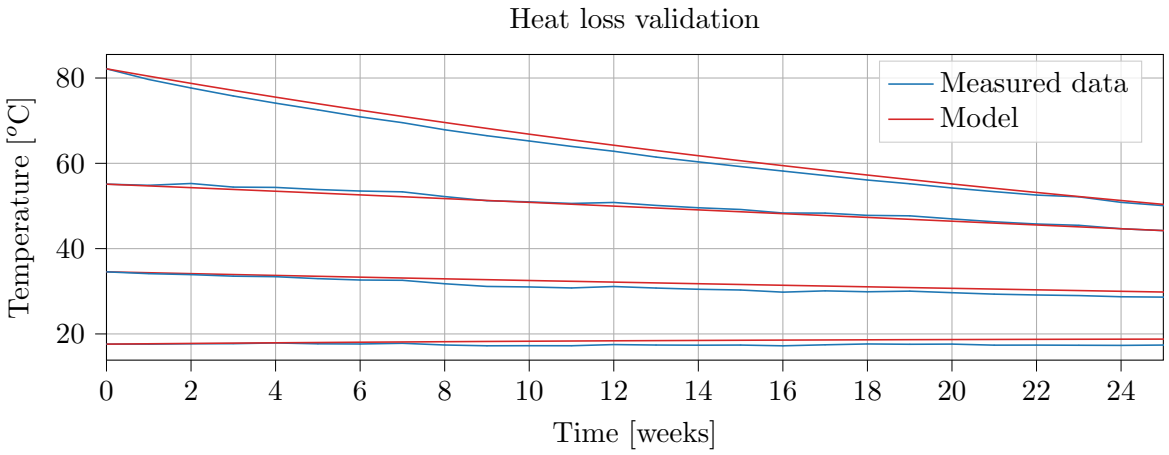

Figure 4.8: Temperature profile of the measured data obtained from heat loss experiments at the Ecovat storage tank in Uden and the model.

4.7.2 Charging

In the past few years, Ecovat took part in the 'Flexible Heat and Power (FHP)' Horizon 2020 project, initiated by the European Union (Mazairac, 2019). For this project, the Ecovat storage tank in Uden is charged a couple of times at the end of 2019. This data is used for the validation of charging an Ecovat storage tank. The measurement data was obtained from 1st August 2019 until 31rd December 2019. It results in multiple sets of measured parameters, including the power input for the WWHPs and AWHPs, as well as the temperatures in the tank. The power inputs are visualised in Figure 4.9.

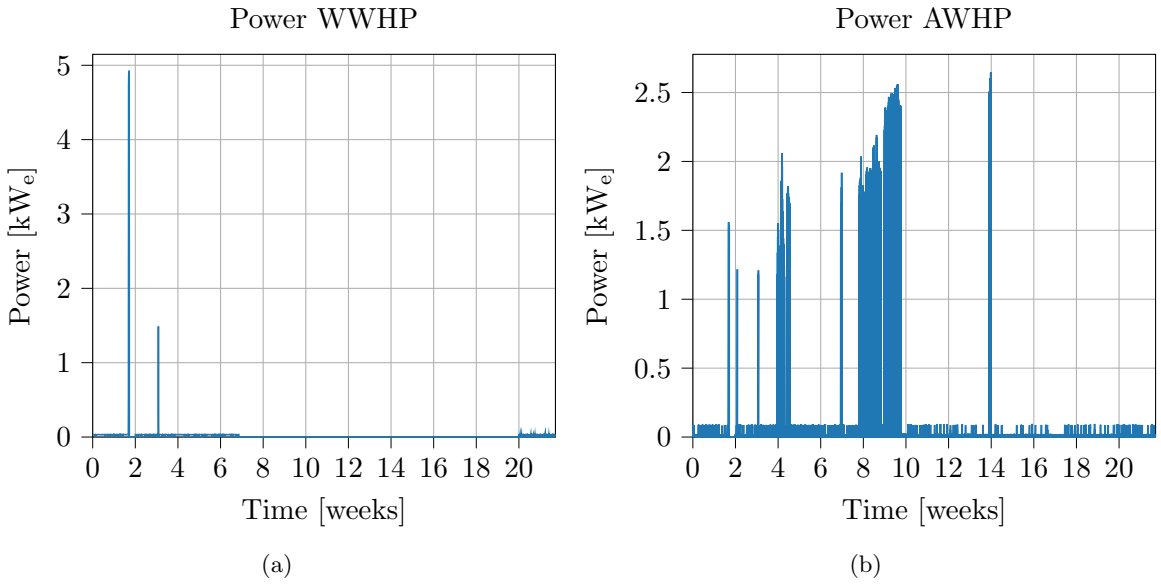

Figure 4.9: Electric power for the (a) WWHPs and (b) AWHPs during the FHP Horizon 2020 project. These charging profiles are used as input for the validation of the model.

The temperature profiles included in this data set are not corrected for the water level, as is the case for the data used in the heat loss validation. During the time of these heat loss measurements, the water level was measured weekly, which was not done during these measurements. However, the change in water level does influence the data. Therefore, an additional assumption is included to deal with this influence, leading to higher uncertainty in the measured data. It is expected that the groundwater level rises in the later months of the measurement period. This hypothesis is approved when looking at the neighbouring groundwater measuring points. All of the checked measuring points show an increase in water level (Provincie Noord-Brabant, 2020). These groundwater measuring locations are, nonetheless, too far away to directly use within the charging validation. Using this knowledge, a difference of water in the same order as Figure 4.7 is expected. Taking a maximum water level difference of $\pm$ 0.5 [m] along the total height of 13.91 [m] and a maximum temperature difference of 20 [°C] with a linear temperature distribution assumed, an additional uncertainty of $\pm$ 1.5 [°C] on the temperature data is taken into account. Again, including the uncertainty of 0.1 [°C] from the temperature sensors a combined uncertainty of $\pm$ 1.5 [°C] is obtained.

Another addition, compared to the validation of the heat loss is the inclusion of the COP values for the AWHPs and WWHPs. EPIC only stores the electrical power used by the heat pumps and not the thermal energy going into the tank. Therefore, the COP values are validated as well. These are set to a constant value 2.4 for the AWHPs and 3.0 for the WWHPs.

To conclude, the validation of the charging temperature data over the August to December period is presented in Figure 4.10. It is observed that the model its temperature profile often lays within the uncertainty boundaries of the measured data. Especially the general shape of the profile follows the data well. However, it is also observed that not all modelled temperatures lay within the uncertainty ranges, which is undesired for validation. The temperatures exceeding the uncertainty ranges are justified by the fact that the model assumes constant COP, whereas this is not the case, in reality, as it depends on the working temperatures of the heat pumps. Moreover, it is observed that the temperatures for the top two layer of the model have similar values, whereas this is not the case for the measured data. During the validation process, it was observed that a higher COP value for the AWHP would increase the temperature difference between these two top layers. Therefore, a variable COP value is stated as a future improvement of the model. Nevertheless, the model in its current form is stated to be accurate enough for this study.

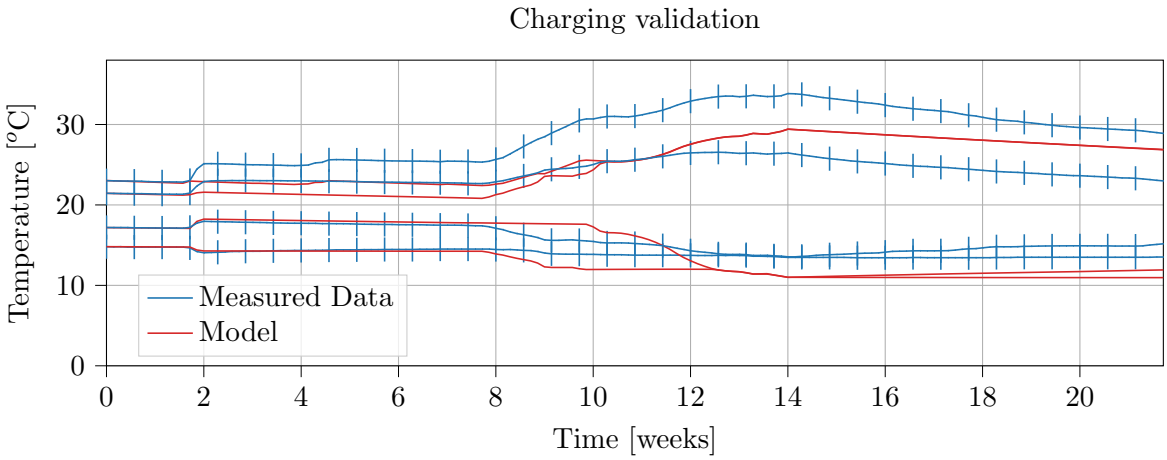

Figure 4.10: Temperature profile of the measured data obtained from charging experiments at the Ecovat storage tank in Uden and the model.

4.8 Convergence

In order to choose the number of layers and time steps when solving the model, it is essential to conduct a convergence study. A convergence study is included to ensure that the results are not affected by changing the time step or number of discretised layers. The convergence study is performed on a two-week basis, instead of a full year. Optimising over a full year with small time steps and a high number of layers is too computational heavy. The obtained convergence plots are presented in Figure 4.11. For this study, it is decided to use a time step of 15 [min] and 16 layers (indicated by the black dots in Figure 4.11).

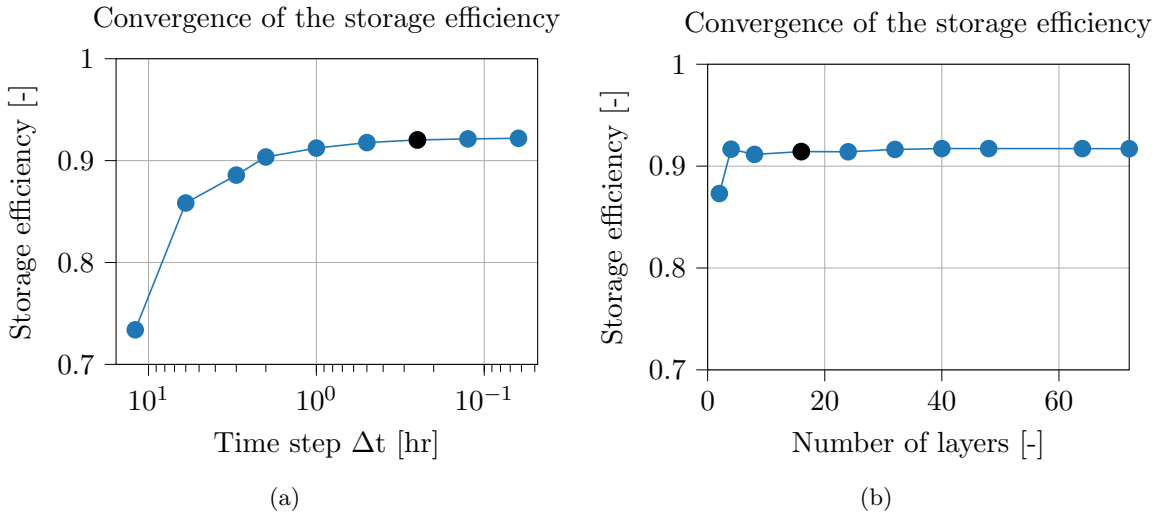

Figure 4.11: (a) Storage efficiency for different time steps in [hr] for a fixed number of layers. (b) Storage efficiency for different number of layers with a constant time step of 15 [min].

4.9 Model Discussion

Before obtaining results, a discussion about the model its limits is inserted. This section elaborates on known shortcomings, model improvements and their expected effects on the results.

First, increasing the number of layers and decreasing the time step, sized up the optimisation problem, resulting in increased computation time. Therefore, the model runs slower than expected. Different solvers for the optimisation algorithm are available with the potential to speed up the model; however, these are only commercially available.

In addition, the diffusers are not yet implemented to the desired level, no circulation of water is taken into account yet. Now, the diffusers only limit the layers in which heat can be injected or extracted and are treated as heat exchangers with no mass flowing in- of out the tank. The heat transfer between water layers is thus merely depended on conduction and therefore still too similar to the Ecovat storage tank in Uden. A start is made to implement the mass flows, accordingly. Nevertheless, it is not yet implemented due to time reasons and the complexity in combination with the optimisation algorithm. To include these mass flows, an additional term representing the heat accompanying the mass flow from one layer to another must be implemented within the energy balance, therefore Equation 4.3 becomes,

$$T(t) = T(t-1) + \frac{1}{\rho_{\mathrm{w},n} V_n c_{\mathrm{p},n}} (q_{\mathrm{charge},\,n,\,t-1} - q_{\mathrm{discharge},\,n,\,t-1} + q_{\mathrm{exchange},\,n,\,t-1} - q_{\mathrm{loss},\,n,\,t-1} + q_{\mathrm{flow},\,n,\,t-1}) \Delta t, \quad (4.16)$$

where $q_{\mathrm{flow},\,n,\,t-1}$ is the heat accompanying the mass flow in from and to neighbouring layers of n at time t-1 in [$\mathrm{kW_{th}}$].

The value for q_{flow} is not non-zero for every layer, however, heat is only transferred between layers that lay within the circulation zone, the region between active diffusers. The additional heat transfer term for layers that do lay within the circulation zone, is denoted as follows,

$$q_{\mathrm{flow,\,n,\,t\text{-}1}} = \dot{m} c_{\mathrm{p}} (T_{n+1}(t-1) + T_{n-1}(t-1) - 2T_n(t-1)), \quad (4.17)$$

where $\dot{m}$ is the mass flow in [kg/s].

This shortcoming of the model might result in an overestimation of the stratification of layers, compared to when circulation zones are included. Therefore, the addition of these mass flow-related terms is recommended as future work.

Finally, the use cases are designed in a way that heat pumps can only supply heat to the storage tank and not directly to the dwellings. Therefore, it is modelled that all heat from the heat pumps flows through the tank before being used within the dwellings, introducing unnecessary losses. Additionally, this causes more heat to be exchanged with the tank than might be necessary. This additional heat exchanged results in a higher CN for an equal amount of dwellings, thus underestimating the maximum number of dwellings that can be provided by the Ecovat storage tank. For future work, more complex use cases should be tested where heat is possible to flow directly from heat pumps to dwellings.

Chapter 5

Optimised Charging and Discharging Profiles

This chapter presents the optimised charging and discharging profile for the seasonal- and peak buffer use cases. In addition, the corresponding performance indicators, introduced in section 3.3, are compared. The total annual costs and equivalent CO_2 emissions are not only compared between the two use cases but also to a situation where no Ecovat storage tank is present. Therefore the annual costs and equivalent CO_2 emissions while using natural gas for 500 and 2,500 dwellings are calculated in section 5.1. These calculations are followed by the results obtained from the model for both use cases, which are compared in section 5.4. Finally, multiple design improvements and their expected effects on the results are given.

5.1 No Ecovat Case

In order to compare the use cases and analyse the results from a broader perspective, it is chosen to compare the total annual costs and CO_2 emissions for both cases also with a baseline case where no Ecovat storage tank is present. In this case, the costs and emissions are solely based on natural gas usage. The amount of natural gas taken into account is the natural gas used to satisfy the energy demand, as presented in subsection 3.1.2. The costs of the gas usage in the Netherlands depend on the price per cubic meter natural gas used, which are assumed to be constant based on a market price of 0.32 [€/m^3] (Milieu Centraal, 2020). When combining this with the annual consumption, 407.20 [€] per dwelling per year is obtained. For the equivalent CO_2 emissions, the annual consumption is multiplied with the CO_2 emission factor of 1.884 [kg/m^3] (SKAO, 2020). The annual gas costs and CO_2 emissions for 500 and 2,500 dwellings are presented in the overview in Table 5.1.

Table 5.1: Annual gas costs and equivalent CO_2 emissions for natural gas usage when no Ecovat is present.

Dwellings [-]	Annual gas costs [€]	ε_{CO_2} [kton]
500	203,603	1.20
2,500	1,018,016	5.99

5.2 Seasonal Use Case

In the seasonal use case, the maximum heat capacity of the tank is discharged 1.47 times during the period of a year, which is a confirmation of the choice of the number of dwellings as part of the use case. Hence, a CN of 1.47 [-] is in line with the expectations and classifies the system as seasonal energy storage. The total amount of the heat flows are presented in Table 5.2. From this table, it is observed that heat losses from the tank to its surroundings are significantly less than heat charged and discharged into and from the tank. These heat flows result in a storage efficiency of 91.9 [%], which is in line with the efficiency that Ecovat promises to its (potential) customers and is validated by DNV·GL (van den Bosch, 2019). Based on the storage efficiency and the CN, it is concluded that the tank design in the use case efficiently can be used as seasonal thermal energy storage.

The optimised charging and discharging profile are presented in Figure 5.1 and Figure 5.2, respectively, which result in a temperature profile, as shown in Figure 5.3. From the charging and discharging profile, various observations are made. First, it is observed that during the colder months, the tank is almost continuously charged with 1,200 [kW_{th}]. This profile is obtained due to the high heat demand during these colder months in combination with the way the use cases are designed, for which no heat can directly be supplied to the dwellings but first must be inserted to the storage tank. Therefore, to satisfy the heat demand, the heat pumps are operating, as only a little heat is charged using solar collectors and residual heat, resulting in total annual full load hours of 259 [hr] for the WWHPs and 3,361 [hr] for AWHPs. Operating the heat pumps in such way as presented in the charging profile, results in 0.89 [kton] equivalent CO_2 emissions and 78,595 [€] electricity costs. Second, it is observed that the charging profile during the summer months is more depended on the solar irradiance profile. During these warmer months, the heat demand from the tank is less and more heat overshoots the directly supplied demand. Therefore, the storage tank is charged, increasing the temperature. Moreover, during these summer months, no additional heat from heat pumps is necessary, which results in no additional electricity costs and CO_2 emissions.

Table 5.2: Annual heat flows for the seasonal use case.

Heat flow	[MWh]
$Q_{discharged}$	4,867
$Q_{charged}$	5,239
Q_{loss}	-427
Q_{init}	1,601
Q_{term}	1,545

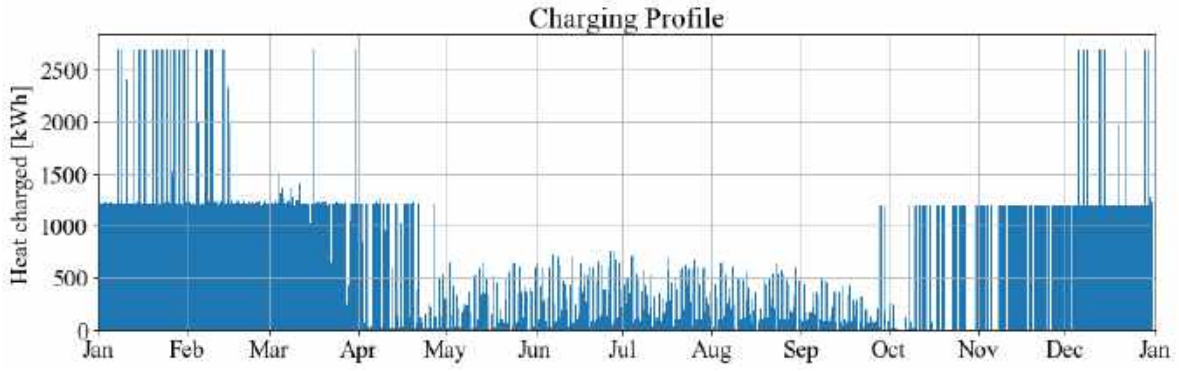

Figure 5.1: Charging profile of the Ecovat storage tank supplied by the solar collectors, residual heat, and heat pumps for the seasonal use case.

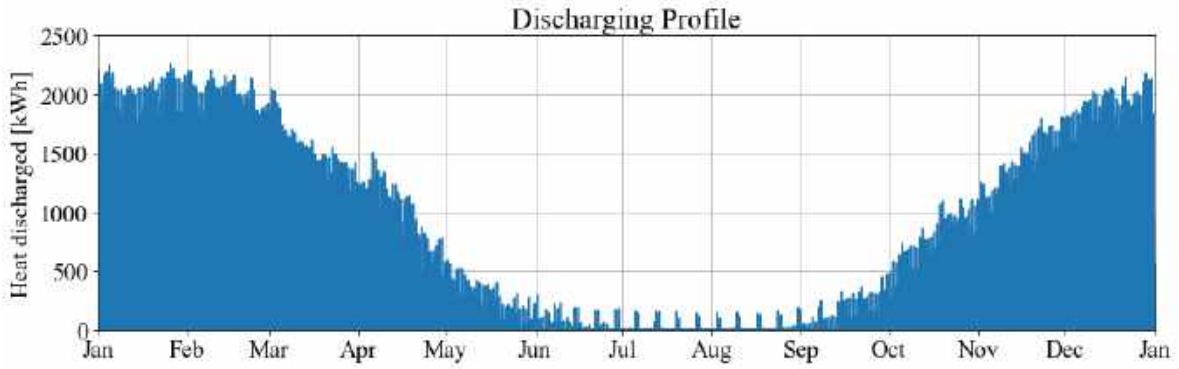

Figure 5.2: Discharging profile of the Ecovat storage tank provided to the dwellings for the seasonal use case.

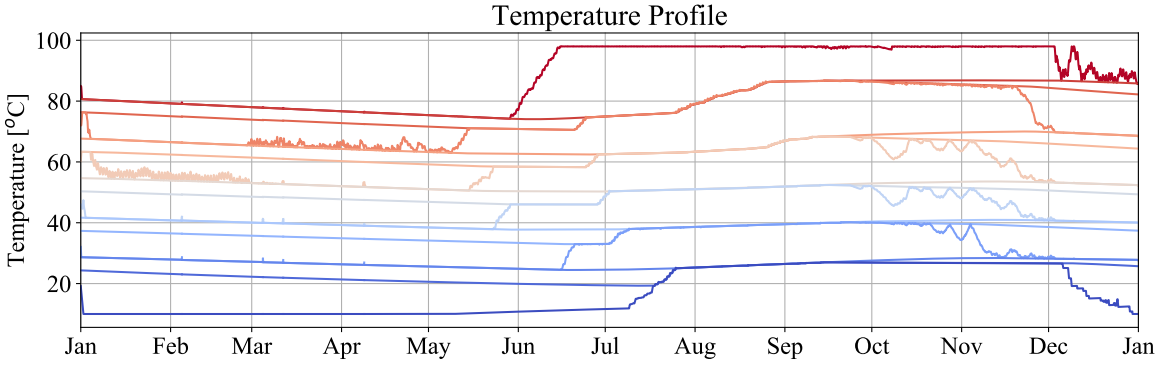

Figure 5.3: Temperature profile for each of the discretised layers for the seasonal use case.

5.3 Peak Buffer Use Case

In the buffer use case, the Ecovat storage tank its maximum heat capacity is discharged 9.42 [-] times during the period of a year. This CN is not closely equal to a day-to-night peak buffer; however, the CN approaches a monthly buffer tank. The storage efficiency for this use case equals 98.8 [%], which has two main causes. First, the heat is not stored at high temperatures for a long period of time, causing little conductive heat losses. Second, the losses are less significant compared to the total discharged heat, which is observed from the total amount of the heat flows that are presented in Table 5.3.

The optimised charging and discharging profiles are presented in Figure 5.4 and Figure 5.5, respectively, which result in a temperature profile, as shown in Figure 5.6. From the charging and discharging profile, various observations are made. It is observed that charging and discharging in the way presented, results in a temperature profile where temperatures often vary, i.e. not showing a gradual seasonally temperature in- or decrease. Moreover, it is observed that the heat pumps are mainly operating at full load during the colder months, correlating to a total of 4,079 full load hours for the AWHPs and 805 for the WWHPs. An exception to this behaviour is observed at the start of June when both the AWHPs and WWHPs operate on full load. This moment correlates to the negative electricity price as presented in Figure 3.3. Operating the heat pumps in a way as presented in the charging profile for the buffer case results in equivalent CO_2 emissions of 5.83 [kton] and electricity costs of 512,719 [€], which results in a total annual cost of 1,056,584 [€] when combined with the costs presented in subsection 3.3.4.

Table 5.3: Annual heat flows for the peak buffer use case.

Heat flow	[MWh]
$Q_{discharged}$	31,230
$Q_{charged}$	31,304
Q_{loss}	-389
Q_{init}	1,601
Q_{term}	1,286

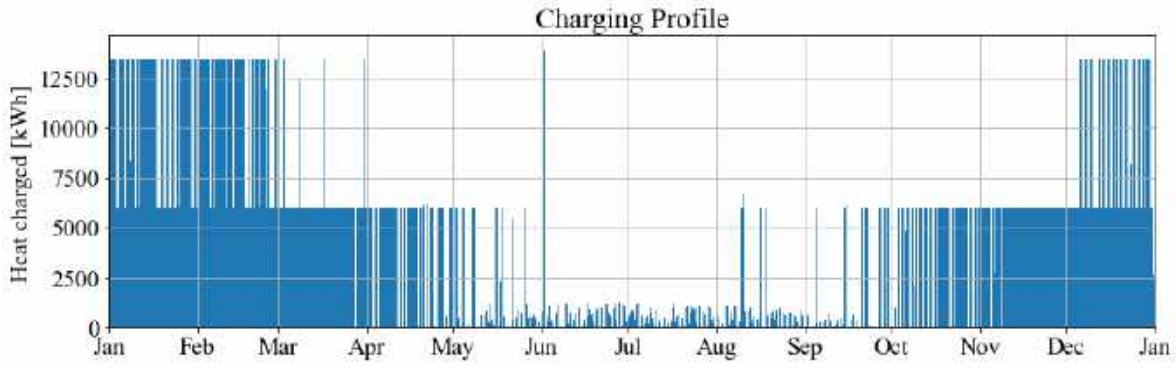

Figure 5.4: Charging profile of the Ecovat storage tank supplied by the solar collectors, residual heat, and heat pumps for the buffer use case.

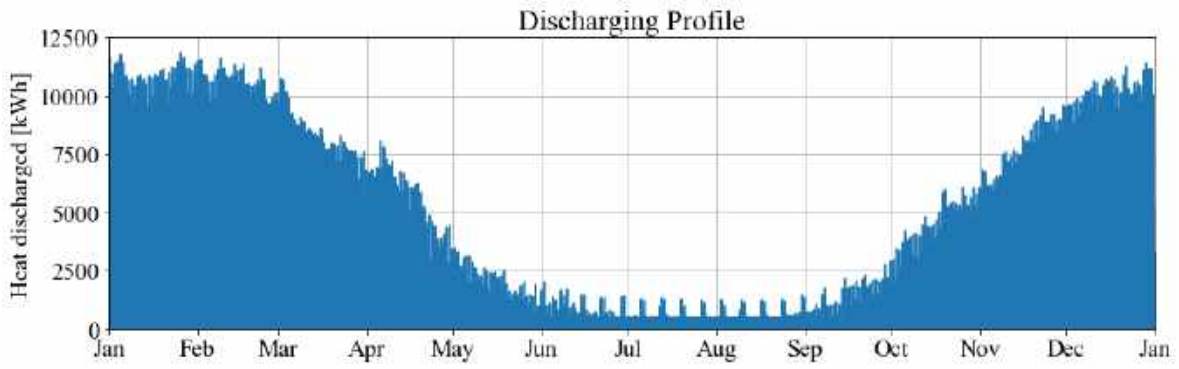

Figure 5.5: Discharging profile of the Ecovat storage tank provided to the dwellings for the buffer use case.

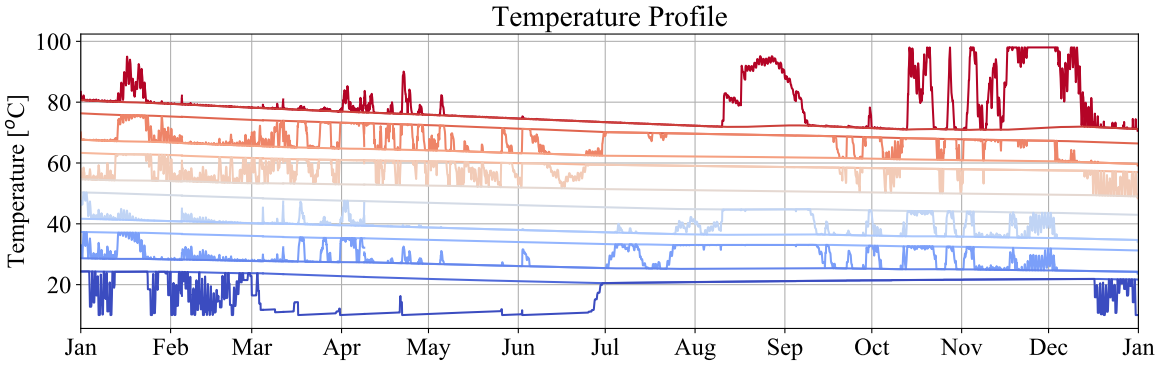

Figure 5.6: Temperature profile for each of the discretised layers for the buffer use case.

5.4 Results Comparison

The results presented in section 5.2 and section 5.3, are summarised and combined in Table 5.4. When comparing the results, it is observed the storage efficiency is 7.0 [%] higher for the peak buffer than for the seasonal use case. This difference is explained due to that heat is stored at a high temperature, $\approx$98 [°C], for a longer period of time during which a rather high amount of heat is lost for the seasonal use case. When comparing this to the temperature profile of the buffer use case, it is observed that this is not the case, thus resulting in fewer heat losses during storage. Moreover, due to the CN being 6.5 times higher for the peak buffer than the seasonal use case, more heat is discharged over a period of time, making the storage losses less significant.

Table 5.4: Overview of the performance indicators for the use cases.

	Dwellings [-]	CN [-]	η [%]	ε_{CO_2} [kton]	Total annual costs [€]
Seasonal case	500	1.47	91.9	0.89	381,927
Peak buffer case	2,500	9.42	98.9	5.83	1,056,584

The equivalent CO_2 emissions and annual costs are not only compared for both use cases but also with the situation where no Ecovat is present. The equivalent CO_2 emissions show a reduction of 26.1 [%] and 2.7 [%] for the seasonal- and buffer use case, respectively, compared with the no Ecovat situation. These relatively low CO_2 reductions, e.g. compared to a completely CO_2 free system with a reduction of 100 [%], are explained by various reasons. The percentage of heat gained by means of heat exchangers is high, which use electricity where the source is unknown rather than 'greener' sources. In addition, heat from heat pumps is not directly supplied to the dwellings, which causes unnecessary storage losses. Therefore, a further reduction of equivalent CO_2 emissions can be realised by including more sustainable energy sources as a heat source, taking electricity from a 'greener' source that emits less CO_2 per kilowatt-hour, and use the heat pump to provide the heat demand directly.

The total annual costs increase 87.6 [%] and 3.8 [%] for the seasonal- and buffer use case, respectively, compared to the annual gas costs, showing that the reduction in equivalent CO_2 emissions does not come without a price. Comparing the total annual costs per dwelling, 763.85 [€] for the seasonal case and 422.63 [€] for the buffer case, it is concluded that the annual costs are 44.7 [%] lower for the buffer than the seasonal use case. These percentages are mainly explained due to the Capex of the Ecovat storage tank being financed by five times as many dwellings and 50 [%] less residual heat and solar collectors per dwelling.

Summarising the comparison, results in the following overview:

- The storage efficiency is 7.0 [%] higher for the peak buffer than for the seasonal use case;
- The CN is 6.5 times higher for the peak buffer than the seasonal use case;
- A reduction of 26.1 [%] and 2.7 [%] in equivalent CO_2 emissions is obtained for the seasonal- and buffer use case, respectively, when compared to the annual CO_2 emissions of natural gas;
- An increase of 87.6 [%] and 3.8 [%] in total annual costs are obtained for the seasonal- and buffer use case, respectively, when compared to the annual gas costs;
- The total annual costs for a dwelling in the buffer use case are 44.7 [%] less than for the seasonal use case.

When combining the above-stated observations with the performance indicators, presented in Table 5.4, it is concluded that the Ecovat storage tank is suitable as buffer storage with a CN of 9.42 [-], which approaches a monthly discharged buffer tank.

5.5 Suggested Improvements

In section 5.4, it is concluded that the Ecovat is to a certain extent suitable as a buffer storage tank. However, the total annual costs are higher than the annual gas costs when no Ecovat is present, and the equivalent CO_2 emission reduction is not as high as for the seasonal use case. Therefore, some possible design improvements are stated, and their possible effects are discussed below.

Over-insulated

From the results of the buffer use case, it became apparent that the storage efficiency equals 98.8 [%]. Therefore, it is suggested that the tank is over-insulated for using the Ecovat storage tank as buffer storage. By decreasing the insulation, a reduction in Capex of the Ecovat storage tank is achieved. However, decreasing the insulation also leads to an increase in heat losses, thus decreasing in storage efficiency. Therefore, it is recommended to research the effects of the percentage by which the Capex can be reduced compared to the additionally obtained heat losses.

Different h/d-ratio, equal volume

In section 2.3, it is discussed that lower h/d-ratios than the ideal ratio of 1.0 [-] are used for the storage tanks in Friedrichshafen, Hanover and Munich due to economic considerations. The Ecovat storage tank included in the use cases has an h/d-ratio of 0.9 [-]. Therefore, for future work, it is recommended to study the effects on the performance indicators when changing the h/d-ratio whilst keeping the volume constant.

Possibilities to reduce equivalent CO_2 emissions

The reduction in equivalent CO_2 emissions equal 26.1 [%] and 2.7 [%] for the seasonal- and buffer use case, respectively, compared to the annual gas costs, leaving room for improvement. The charging and discharging profiles, presented in section 5.2-5.3, show that heat is mainly generated by the heat pumps during the colder month, limiting the emission reduction. Therefore, various suggestions are made to reduce the equivalent CO_2 emissions. First, introducing an additional sustainable energy source by including electricity from wind turbines enables the heat pumps to operate on electricity that emits less CO_2 per kilowatt-hour. Moreover, by finding an industry that has an increased residual heat in the colder months, thus following demand profile better rather than being constant during the year, the operational hours of the heat pumps can be reduced. However, if such profiles exist requires additional research on the availability of residual heat.

Chapter 6

Conclusions & Recommendations

This chapter evaluates the research questions formulated in section 1.2. In addition, recommendations regarding future work and the suitability of the Ecovat storage tank as buffer storage are presented.

6.1 Conclusion

The similarities and differences between typical seasonal- and buffer TTES systems are described by comparing the seasonal heat storages in Friedrichshafen, Hanover, and Munich to buffer heat storages in Linz, Duisburg, Theiß, Diemen, and Angeli di Rosora. The comparison shows that seasonal storage tanks have an h/d-ratio lower than 1.0 [-] whereas buffer tanks generally have h/d-ratios higher than 1.0 [-]. Both h/d-ratios are based on the efficiencies and costs for their designed operation. Additionally, it is observed that seasonal storage tanks have concrete as the primary material, either existing of high-quality concrete or concrete with a stainless steel liner, compared to buffer storage tanks which mostly use steel. Moreover, the location of both types of storage tanks is different. The seasonal tanks are buried underground in residential areas whereas the buffer tanks are located above-ground near industry. Next to these differences, a tank characteristic that is similar for both types of storage tanks relates to the heat capacity. The heat capacity of a tank is based on the available heat sources, i.e. a high amount of residual heat or a limited number of solar collectors, and the desired heat demand.

Based on the comparison, two use cases are designed, one for a situation where the Ecovat storage tank is used as seasonal storage and one where it is used as buffer storage. The use cases consist out of several system components with the Ecovat storage tank as the main component. Both use cases include the same Ecovat storage tank design with a height of 32.4 [m] and a diameter of 36.0 [m], resulting in an h/d-ratio of 0.9 [-] and a volume capacity of 32,979 [m^3]. Solar collectors, residual heat and heat pumps are used as heat sources, and heat demand of 500 and 2,500 dwellings are included in the use cases.

Different performance indicators are used to compare the performance of an Ecovat storage tank for both use cases, consisting of the cycle number, storage efficiency, equivalent CO_2 emissions, and annual costs. In order to obtain values for these indicators, a model is presented. This model represents the stratified Ecovat storage tank and is discretised in cylindrical

shaped layers to take the buoyancy effects into account. Each of the layers has a homogeneous temperature which depends on its energy balance. The change of energy of a discretised layer is solely depended on the addition or removal of heat, which is based on the heat sources and demand included in the use cases. Most of these terms have a known profile, i.e. the solar collectors based on the irradiance profile, a constant residual heat, and heat demand based on the annual gas usage, however, the charging profile regarding the heat pumps is solved during the optimisation process. Therefore, to get an optimal charging and discharging strategy for each of the use cases, the electricity costs to operate heat pumps are minimised. In order to minimise these electricity costs, the energy balance is included within a convex optimisation model, which is solved using the ADMM algorithm. This convex optimisation model is successfully validated against experimental data obtained from the Ecovat storage tank in Uden.

Solving the convex optimisation model for a year, showed that both, the seasonal- and buffer use cases reduce the annual equivalent CO_2 emissions compared to what has been emitted if natural gas is used to satisfy the heat demand. However, both also show that the total annual costs increase compared to natural gas. It is observed that the seasonal use case results in a storage efficiency of 91.9 [%] and CN of 1.47 [-]. Comparing these performance indicators to a storage efficiency of 98.8 [%] and CN of 9.42 [-] for the buffer use case, it is observed that the buffer use case results in a higher storage efficiency and a CN that is around 6.5 times higher than the seasonal use case. Therefore, it is concluded that the Ecovat storage tank is suitable as buffer storage with a CN of 9.42 [-], which approaches a monthly discharged buffer tank.

6.2 Recommendations

Several recommendations are made for both the model, as well as the design of the Ecovat storage tank. The latter primarily focuses on total annual costs reduction possibilities when operating as buffer storage.

6.2.1 Different use cases

In this study, two types of use cases are included, which both include the same system components. It is recommended to expand this set of use cases to create a broader perspective of the possibilities of an Ecovat storage tank. Different use cases can include different components, e.g. including wind turbines, as well as different values for already included components, e.g. increase the area of solar collectors.

6.2.2 Improving model limitations

The model has several known limitations regarding solving speed, implementation of diffusers, and supplying more heat directly to the demand. It is recommended that these limitations are improved for future work. Currently, the convex optimisation makes use of free available solvers. To reduce the solving time, commercially available solvers might be worth looking into. Moreover, no circulation of water is taken into account yet. In order to improve the extent to which diffusers are included in the model, it is recommended to implement water circulation. Finally, it is recommended to enable the model to supply heat from the heat pumps directly to the dwellings to prevent unnecessary losses.

6.2.3 Ecovat storage tank

It is concluded that the Ecovat storage tank with its current design is suitable to be used as buffer storage. However, due to the storage efficiency equalling 98.8 [%], it is suggested that the effects of reducing the insulation create an opportunity to reduce the Capex of an Ecovat storage tank while still being able to reach an acceptable efficiency. Moreover, it is recommended to try different h/d-ratios whilst keeping the volume constant, such that an overview of the most efficient design is obtained for different scenarios.

References

Abdelhak, O., Mhiri, H. & Bournot, P. (2015, August). CFD analysis of thermal stratification in domestic hot water storage tank during dynamic mode. *Building Simulation*, *8*(4), 421–429. doi: 10.1007/s12273-015-0216-9

Automatie-PMA. (2016, November 7). *Speciaal warmtebuffer garandeert stadsverwarming.* Retrieved April 4, 2020, from https://automatie-pma.com/nieuws/speciaal-warmtebuffer-garandeert-stadsverwarming.

Bartels, J. (2019). *APX Prijs 2019* [Data file]. Amstelveen: E.D.Mij B.V.

Bauer, D., Marx, R., Nußbicker-Lux, J., Ochs, F., Heidemann, W. & Müller-Steinhagen, H. (2010). German central solar heating plants with seasonal heat storage. *Solar Energy*, *84*(4), 612 - 623. Retrieved from http://www.sciencedirect.com/science/article/pii/S0038092X09001224 (International Conference CISBAT 2007) doi: 10.1016/j.solener.2009.05.013

Bilfinger SE. (2014). *Hightech für effizientere Strom- und Wärmeversorgung.* Retrieved July 15, 2020, from https://www.bilfinger.com/media/news/hightech-fuer-effizientere-strom-und-waermeversorgung/.

Boffey, D. (2018). *Gas field earthquakes put Netherlands' biggest firms on extraction notice.* Retrieved from https://www.theguardian.com/environment/2018/jan/23/gas-field-earthquakes-put-netherlands-biggest-firms-on-extraction-notice.

Bott, C., Dressel, I. & Bayer, P. (2019). State-of-technology review of water-based closed seasonal thermal energy storage systems. *Renewable and Sustainable Energy Reviews*, *113*, 109241. Retrieved from http://www.sciencedirect.com/science/article/pii/S1364032119304411 doi: 10.1016/j.rser.2019.06.048

Boyd, S. & Vandenberghe, L. (2004). *Convex optimization.* Cambridge University Press.

Comodi, G., Giantomassi, A., Severini, M., Squartini, S., Ferracuti, F., Fonti, A., ... Polonara, F. (2015). Multi-apartment residential microgrid with electrical and thermal storage devices: Experimental analysis and simulation of energy management strategies. *Applied Energy*, *137*, 854–866. doi: 10.1016/j.apenergy.2014.07.068

Dahash, A., Ochs, F., Janetti, M. B. & Streicher, W. (2019). Advances in seasonal thermal energy storage for solar district heating applications: A critical review on large-scale hot-water tank and pit thermal energy storage systems. *Applied Energy*, *239*, 296 - 315. doi: 10.1016/j.apenergy.2019.01.189

de Energiemanager. (2020). *Standaard verbruiksprofielen aardgas.* Retrieved May 14, 2020, from http://www.deenergiemanager.nl/tools/P_aardgas.html.

de Ridder, F. & Mazairac, W. (2019). *Reliance report.* (Not publicly available)

de Groot, S. (2020). *Comparison of Ecovat to large, seasonal, sensible, thermal energy storage technologies for district heating networks.* Retrieved from

https://www.ecovat.eu/wp-content/uploads/2020/06/20200609-Ecovat_comparison_Final_ENG-gecomprimeerd.pdf.

Diamond, S. & Boyd, S. (2016). CVXPY: A Python-embedded modeling language for convex optimization. *Journal of Machine Learning Research*, *17*(83), 1-5.

Diamond, S., Chu, E. & Boyd, S. (2020). *Disciplined Convex Programming.* Retrieved June 23, 2020, from https://dcp.stanford.edu/.

Energievergelijken.nl. (n.d.). *Gemiddeld gasverbruik.* Retrieved May 14, 2020, from https://www.energievergelijken.nl/gas/gemiddeld-gasverbruik.

EVN. (n.d.). *Fernwärmespeicher Theiß.* Retrieved February 26, 2020, from https://www.evn.at/Privatkunden/Waerme/EVN-Waerme-GmbH/Projekt-Thei%C3%9F.aspx.

GEA. (2018). *Heatpump comparison tool - prices.* (Internal tool, not publicly available)

Gimmelsberger, J. (2004, October 21-22). Efficient energy supply (electricity and district heat) for the city of Linz [Paper presentation]. In *Energy Efficiency in IPPC installations - European Conference* (p. 91-97). Vienna, Austria.

GoToTanks, Inc. (2018, July 9). *Above ground vs. underground: Where should your water storage tank be positioned?* Retrieved March 7, 2020, from https://gototanks.com/storage-tanks/above-ground-vs-underground-where-should-your-water-storage-tank-be-positioned.html.

Karim, A., Burnett, A. & Fawzia, S. (2018). Investigation of stratified thermal storage tank performance for heating and cooling applications. *Energies*, *11*(5), 1049. doi: 10.3390/en11051049

KNMI. (2019). *Daggegevens van het weer in Nederland.* Retrieved May 14, 2020, from http://projects.knmi.nl/klimatologie/daggegevens/selectie.cgi.

Kolokotsa, D., Kampelis, N., Mavrigiannaki, A., Gentilozzi, M., Paredes, F., Montagnino, F. & Venezia, L. (2019). On the integration of the energy storage in smart grids: Technologies and applications. *Energy Storage*, *1*(1), e50. Retrieved from https://onlinelibrary.wiley.com/doi/abs/10.1002/est2.50 doi: 10.1002/est2.50

Lago, J., De Ridder, F., Mazairac, W. & De Schutter, B. (2019). A 1-dimensional continuous and smooth model for thermally stratified storage tanks including mixing and buoyancy. *Applied Energy*, *248*, 640 - 655. Retrieved from http://www.sciencedirect.com/science/article/pii/S0306261919307901 doi: 10.1016/j.apenergy.2019.04.139

Ledyard, J. & Chandy, M. (2005, January). *Fundamental Theorems of Optimization* [PowerPoint Slides] . Caltech Institute of Technology. Retrieved from http://courses.cms.caltech.edu/cs101b/lectures/lecture2.pdf.

Leitner, S. (2013). *Physik neuartiger Wärmespeicher* (Doctoral dissertation, Universität Wien). Retrieved from http://othes.univie.ac.at/25875/1/2013-01-30_9171430.pdf. doi: 10.25365/thesis.25875

Lemmens, J., Beurskens, L. & Lensink, S. (2020, May 7). *Conceptadvies SDE++ 2021 zonne-energie* (Productnummer 4104). Retrieved from https://www.pbl.nl/publicaties/conceptadvies-sde-2021-zonne-energie.

Linz AG. (n.d.). *Fernheizkraftwerk Linz-Mitte.* Retrieved July 15, 2020, from https://www.linzag.at/portal/de/ueber_die_linzag/konzern/gesellschaften/linz_strom_gas_waerme_gmbh/energieerzeugung/fernheizkraftwerk_linz_mitte#.

Lousberg, J. (2014). *Warmtebuffer Diemen bereikt hoogste punt* [Photograph]. Retrieved from https://www.flickr.com/photos/vattenfall_nederland/15950172977.

Mangold, D. (2006, November 2-3). Saisonale Wärmespeicher: neue Pilotanlagen im Programm Solarthermie2000plus und Forschungperspektiven. In *Statusseminar Thermische*

Energiespeicher. Freiburg, Germany.

Mangold, D. (2007). Seasonal Storage - a German success story. *Sun & Wind Energy*, *1*, 48-55.

Mangold, D. & Peuser, F. (2003, June 14-19). Solarthermie-2000: 10 Years of research and development in large solar heating systems in Germany. In *ISES Solar World Congress 2003.* Göteborg, Sweden.

Mazairac, W. (2019). *Flexible heat and power, connecting heat and power networks by harnessing the complexity in distributed thermal flexibility.* Retrieved from http://fhp-h2020.eu/wp-content/uploads/2020/02/D4.3-Ecovat-validation.pdf.

Milieu Centraal. (2020). *Grip op je energierekening.* Retrieved September 17, 2020, from https://www.milieucentraal.nl/energie-besparen/snel-besparen/grip-op-je-energierekening/energierekening/.

Ministerie van Economische Zaken. (2016, December 7). *Energieagenda - Naar een CO_2-arme energievoorziening.* Retrieved from https://www.rijksoverheid.nl/documenten/rapporten/2016/12/07/ea.

Muller, M. & Lensink, S. (2020, May 7). *Conceptadvies SDE++ 2021 Benutting restwarmte uit industrie of datacenters* (Productnummer 4113). Retrieved from https://www.pbl.nl/publicaties/conceptadvies-sde-2021-benutting-restwarmte-uit-industrie-of-datacenters.

Nibud. (2020). *Energie en Water - Gasverbruik.* Retrieved May 14, 2020, from https://www.nibud.nl/consumenten/energie-en-water/.

Niessink, R. (2020, April 17). *Heat networks low temperature households (district heating).* Retrieved September 2, 2020, from https://energy.nl/en/fact_sheet/low-temperature-heat-networks-district-heating/.

Njoku, H., Ekechukwu, V. & Onyegegbu, S. (2014). Analysis of stratified thermal storage systems: An overview. *Heat and Mass Transfer*, *50*, 1017-1030. doi: 10.1007/s00231-014-1302-8

Oberhammer, A. & Prawits, T. (2012, March 22). Fernwärmespeicher: Bauarten, Auslegung und Beispiele [PowerPoint presentation]. Retrieved from https://web.archive.org/web/20131228045526/http:/www.gaswaerme.at/de/pdf/12-1/oberhammer.pdf.

Ochs, F. (2013). *Stand der Technik erdvergrabener Wärmespeicher.* Retrieved from http://www.aee-now.at/cms/fileadmin/downloads/projekte/store4grid/store4grid_stand_der_technik.pdf.

Ochs, F., Heidemann, W. & Müller-Steinhagen, H. (2009). Performance of Large-Scale Seasonal Thermal Energy Stores. *Journal of Solar Energy Engineering*, *131*(4). Retrieved from https://asmedigitalcollection.asme.org/solarenergyengineering/article-pdf/131/4/041005/5700889/041005_1.pdf doi: 10.1115/1.3197842

PDHU. (2017). *A revolutionary idea.* Retrieved from https://www.westminster.gov.uk/yourhousing/sites/default/files/documents/2017-06/Pimlico%20District%20Heating%20Undertaking%20factsheet.pdf

Provincie Noord-Brabant. (2020). *Grondwaterstanden en -meetnetten.* Retrieved May 3, 2020, from https://grondwaterstand.brabant.nl.

Raab, S., Mangold, D. & Müller-Steinhagen, H. (2005). Validation of a computer model for solar assisted district heating systems with seasonal hot water heat store. *Solar Energy*, *79*(5), 531 - 543. Retrieved from http://www.sciencedirect.com/science/article/pii/S0038092X05000289 doi: 10.1016/j.solener.2004.10.014

Rijvers, L., Rindt, C. & de Keizer, C. (2020). *Design and analysis of a residential energy system that integrates hybrid solar modules (PVT) with a heat pump.* (PDEng Report, Eindhoven University of Technology)

Schepers, B. & van Lieshout, M. (2011). *IPO Nationale Routekaart Restwarmte.* Retrieved from https://www.ce.nl/publicatie/ipo_nationale_routekaart_restwarmte/1164

sdg21. (2016, August 15). *Solare Nahwärme Ackermannbogen.* Retrieved February 21, 2020, from https://siedlungen.eu/db/solare-nahwaerme-ackermannbogen.

SIKA. (n.d.). *Präzisionsthermometer MH3710: Bedienungsanleitung.*

SKAO. (2020). *Lijst emissiefactoren.* Retrieved July 9, 2020, from https://www.co2emissiefactoren.nl/lijst-emissiefactoren/.

Solaris. (n.d.). *Projekte in Deutschland.* Retrieved March 5, 2020, from http://www.saisonalspeicher.de/Projekte/ProjekteinDeutschland.

Stadtwerke-Duisburg. (n.d.). *Der Wärmespeicher der Stadtwerke Duisburg.* Retrieved February 26, 2020, from https://www.stadtwerke-duisburg.de/unternehmen/themen/der-waermespeicher-der-stadtwerke-duisburg/.

Stratelligence. (2020, April 3). *Een Laagdrempelige Energietransitie.* Retrieved from https://www.energie-nederland.nl/app/uploads/2020/04/Laagdrempelige-energietransitie-stratelligence-3-april-1.2-min.pdf.

United Nations. (2015). *The Paris Agreement.* Retrieved June 3, 2020, from https://unfccc.int/process-and-meetings/the-paris-agreement/the-paris-agreement.

Unsworth, R. & Hoffmann, K. (2020, June 24). *Decarbonize heating processes and reduce operating costs* [Webinar]. GEA. Retrieved from https://www.gea.com/en/events/webinars/industrial-heat-recovery-webinar.jsp.

van den Bosch, R. (2018). *Ecovat - Validation of the thermal efficiency based on the demonstration Ecovat Uden.* (Not publicly available)

van den Bosch, R. (2019). *Ecovat - Productinformatie.* (Not publicly available)

van den Bosch, R. (2020). *Projectbegroting Opex & Capex.* (Not publicly available)

van der Wal, W. (2003). Chapter 2 - The Technological Infrastructure of the Gas Chain. In M. J. Arentsen & R. W. Künneke (Eds.), *National Reforms in European Gas* (p. 13 - 29). Oxford: Elsevier Science. Retrieved from http://www.sciencedirect.com/science/article/pii/B9780080436876500043 doi: 10.1016/B978-008043687-6/50004-3

Vattenfall. (n.d.). *Stadsverwarming uit een thermoskan.* Retrieved February 27, 2020, from https://www.vattenfall.nl/duurzame-energie/stadswarmte/stadsverwarming-uit-een-thermoskan/.

Vincent-Rous, A. (2010). *Pimlico District Heating Undertaking Tower* [Photograph]. Retrieved from https://www.flickr.com/photos/by-jack/4779544287.

Wohlberg, B. (2017). ADMM Penalty Parameter Selection by Residual Balancing. *ArXiv*, *abs/1704.06209*. Retrieved from https://arxiv.org/pdf/1704.06209.pdf

Zondag, H. A. (2019). *Thermal Energy Storage 4EM50 - Course 2018-2019* [Lecture Notes]. Eindhoven University of Technology. Retrieved from https://canvas.tue.nl/.

Appendix A

Cycle Number Calculations

To give a visualisation of the cycle number and help the understanding of the classification between seasonal storage tanks and buffer tanks, Figure 3.5 is included. The literature states only little about the exact number of charging cycles per year, especially for buffer tanks. Therefore, some assumptions made regarding the CN in subsection 3.3.1 are explained within this appendix. For completeness, Equation 3.4-3.5 are given below,

$$\mathrm{CN} = \frac{Q_{\mathrm{discharged}}}{Q_{\mathrm{max}}}, \tag{A.1}$$

$$Q_{\mathrm{max}} = V_{\mathrm{tank}} \rho_{\mathrm{w}} c_{\mathrm{p,w}} \left(T_{\mathrm{max}} - T_{\mathrm{min}}\right). \tag{A.2}$$

where $Q_{\mathrm{discharged}}$ is the total discharged heat in [kWh], Q_{max} the maximum storage capacity in [kWh], V_{tank} the volume of the Ecovat storage tank in [m^3], ρ_{w} the density of water in [kg/m^3], $c_{\mathrm{p,w}}$ the specific heat capacity of water [kWh/(kg K)] and, T_{max} and T_{min} are, respectively, the maximum and minimum temperature in the tank in [°C] over a specified period of time.

To get the total discharged heat, a demand profile, as shown in Figure 3.2 is used, resulting in a heat demand of 12.4 [MWh] per dwelling. Moreover, in section 2.2, it is stated how much dwellings are provided by a particular storage tank, combining these two results in the total heat demand for a system. However, it assumed that the tank supplies not all of the demand, but rather 70 [%]. This percentage is assumed as a total of 100 [%] is unrealistic with the explained working principles and a lower percentage, e.g. 10 - 20 [%], would not be realistic either as this would mean that the storage tank would barely be used. This percentage might differ in reality. Therefore CN is calculated for 50, 70, and 90 [%], from which the middle one is included in the overview. The obtained CN for the buffer tanks in Theiß and Diemen are included in Table A.1.

Table A.1: Cycle number calculations for the storage tanks in Theiß and Diemen.

	Nr. Dwellings [-]	V_{tank} [m^3]	$T_{\mathrm{max}} - T_{\mathrm{min}}$ [°C]	$\mathrm{CN}_{50\%}$ [-]	$\mathrm{CN}_{70\%}$ [-]	$\mathrm{CN}_{90\%}$ [-]
Theiß	5,000	50,000	70	7.76	10.86	13.97
Diemen	75,000	220,000	100	131.10	183.54	235.98

Appendix B

Convex Optimisation

In order to compare optimised charging and discharging behaviour, it is optimised using convex optimisation. The objective function is explained in more detail in this appendix. At the start of this appendix, it is proven that the objective function can be solved using CVXPY. In addition, the conversion to an ADMM compatible objective function is presented. Moreover, the different components of the objective function are validated. In the end, CVXPY is compared to an analytical problem.

B.1 Affine Objective Function

Affine functions are able to be solved using convex optimisation. To prove a function is affine, it must hold that,

$$f(\theta\beta + (1-\theta)\,\gamma) = \theta f(\beta) + (1-\theta)\,f(\gamma), \tag{B.1}$$

$$f(\theta\beta + (1-\theta)\,\gamma) - \theta f(\beta) - (1-\theta)\,f(\gamma) = 0, \tag{B.2}$$

for all β, $\gamma \in \mathbf{R}^p$ and all $\theta \in [0, 1]$ (Diamond, Chu & Boyd, 2020).

Taking the terms within the integral of Equation 4.12, as function, f, results in the following equation,

$$f(P_{\text{grid}}) = c\,P_{\text{grid}}, \tag{B.3}$$

where c are the costs of electricity at a certain moment in time in [€/kWh] presented in Figure 3.3 and $\mathrm{P_{grid}}$ is the electricity supplied by the grid in [$\mathrm{kW_e}$].

Substituting the above stated equation in Equation B.2, results the following,

$$c\,(\theta\beta + (1-\theta)\,\gamma) - \theta c\beta - (1-\theta)\,c\gamma = 0, \tag{B.4}$$

$$c\,(\theta\beta + (1-\theta)\,\gamma) - c\,(\theta\beta + (1-\theta)\,\gamma) = 0, \tag{B.5}$$

which shows that Equation B.3 is affine. Moreover, it is stated that applying an affine expression to affine functions, e.g. taking the sum, results again in an affine function. This shows that the objective function as presented in Equation 4.12 is affine and therefore can be solved using convex optimisation.

B.2 ADMM Compatible Objective Function

The convex optimisation problem can be solved efficiently using the ADMM algorithm. The advantage of solving via the ADMM algorithm is that it speeds up the calculations by breaking the total problem into smaller pieces, as visualised in Figure B.1.

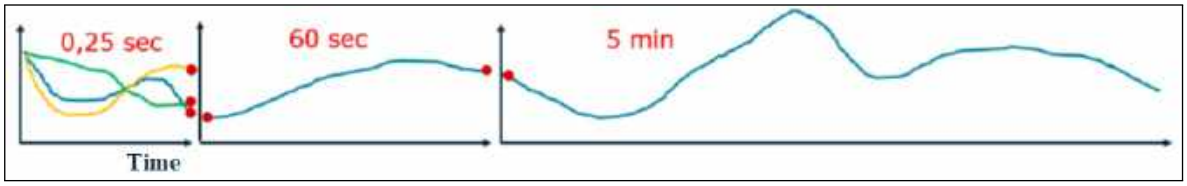

Figure B.1: Examples of computation times (in red) for solving using the ADMM algorithm (de Ridder & Mazairac, 2019).

To make Equation 4.12 compatible such that it can be solved using ADMM, it has to be re-written. Breaking the problem into smaller pieces introduces additional constraints, which creates the following generic problem,

$$\begin{aligned} &\text{minimise} && f(\boldsymbol{x}), \\ &\text{such that} && T_{m,0} - \overline{T}_{\text{init}} = 0, \\ & && T_{m,\text{end}} - \overline{T}_{\text{term}} = 0, \end{aligned} \tag{B.6}$$

where $f(\boldsymbol{x})$ is the objective function which has to be minimised, $\boldsymbol{x}$ is a vector containing the optimisation variables, $T_{m,0}$ and $T_{m,end}$ are the initial and final temperature per layer of the period m, respectively, $\overline{T}_{\text{init}}$ is the average temperature of a layer between the initial temperature of period m and the final temperature of period m - 1, and $\overline{T}_{\text{term}}$ is the average temperature of a layer between the final temperature of period m and the initial temperature of period $m + 1$.

Introducing the Lagrangian parameters λ_{init} and λ_{term} helps relaxing the problem. By relaxing the objective function with these parameters, the Lagrangian for the constrained problem is obtained,

$$L(\boldsymbol{x}, \lambda_{\text{init}}, \lambda_{\text{term}}) = f(\boldsymbol{x}) + \lambda_{\text{init}}(T_{m,0} - \overline{T}_{\text{init}}) + \lambda_{\text{term}}(T_{m,\text{end}} - \overline{T}_{\text{term}}). \tag{B.7}$$

The method of multipliers solves the above stated problem via dual ascent for k ADMM iterations,

$$\boldsymbol{x}^{(k+1)} = \min L_\alpha(\boldsymbol{x}, \lambda_{\text{init}}^{(k)}, \lambda_{\text{term}}^{(k)}) \tag{B.8}$$

$$\lambda_{\text{init}}^{(k+1)} = \lambda_{\text{init}}^{(k)} + \alpha \left(T_{m,0} - \overline{T}_{\text{init}}\right) \tag{B.9}$$

$$\lambda_{\text{term}}^{(k+1)} = \lambda_{\text{term}}^{(k)} + \alpha \left(T_{m,\text{end}} - \overline{T}_{\text{term}}\right), \tag{B.10}$$

where L_α is the augmented Lagrangian and α is the penalty parameter (Wohlberg, 2017).

Combining the dual ascent terms of Equation B.8-B.10 with Equation B.7, results the augmented Lagrangian,

$$\begin{aligned} L_\alpha(\boldsymbol{x}, \lambda_{\text{init}}, \lambda_{\text{term}}) = f(\boldsymbol{x}) &+ \lambda_{\text{init}}(T_{m,0} - \overline{T}_{\text{init}}) + \frac{1}{2}\alpha \left(T_{m,0} - \overline{T}_{\text{init}}\right)^2 \\ &+ \lambda_{\text{term}}(T_{m,\text{end}} - \overline{T}_{\text{term}}) + \frac{1}{2}\alpha \left(T_{m,\text{end}} - \overline{T}_{\text{term}}\right)^2. \end{aligned} \tag{B.11}$$

This augmented Lagrangian becomes the new objective function as presented in Equation 4.13 and is solved using the embedded conic solver (ECOS), an interior-point solver, in the CVXPY software.

B.3 Validating the Objective Function

In order to be confident that the objective function gives the desired results, it is validated on its working. Three parts are identified which are tested separately, minimising the electricity costs, a penalty on unrealistic temperature distributions, and the matching of temperatures of subsequent periods.

First, it is tested if the heat is bought from the grid at the moment the electricity price is low, which is tested using a demand profile, as presented in Figure B.2. Sometime before the peak in the heat demand, a sudden drop in electricity price is introduced. It is observed that this part of the objective function works as designed, as heat is bought when the electricity price is low.

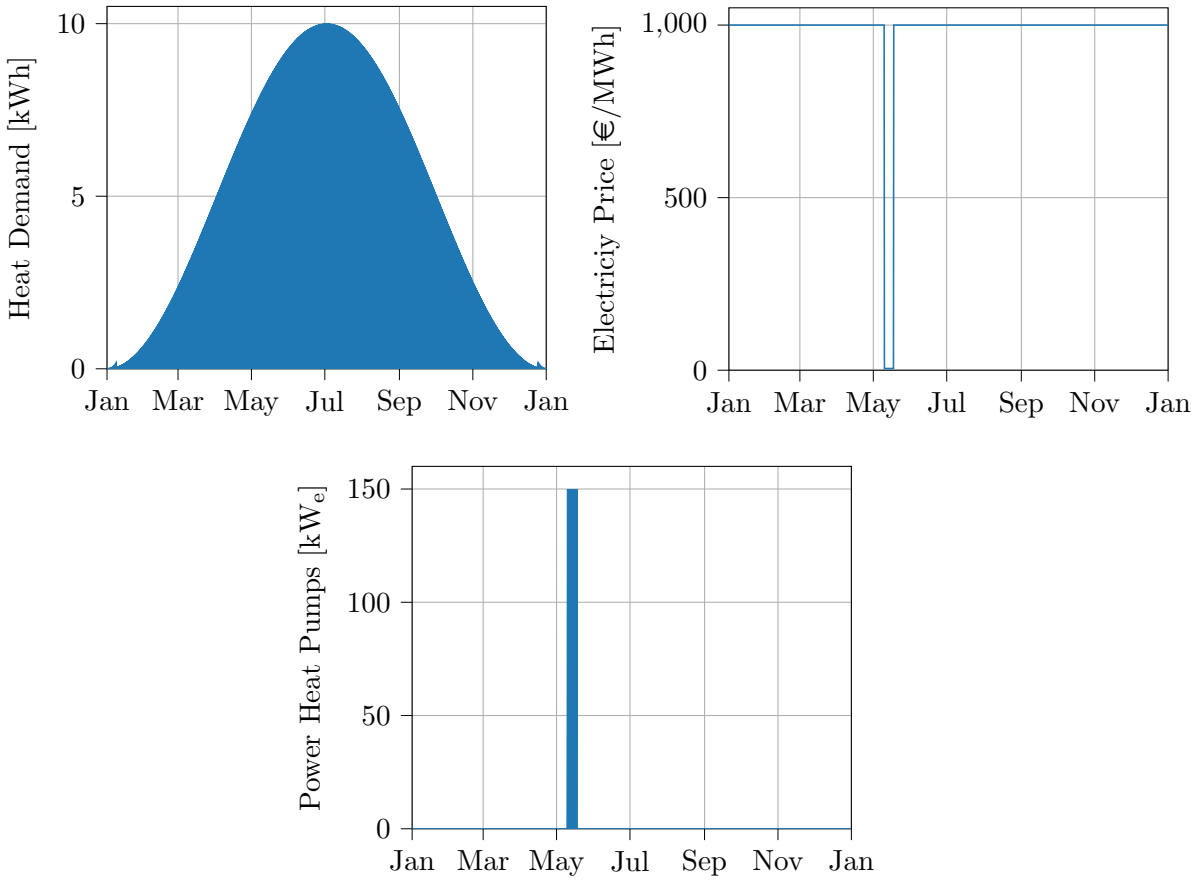

Figure B.2: Testing the objective function on buying electricity on time and when the electricity price is low.

Second, the penalty on unrealistic temperature distributions is tested in section 4.5. There it is shown that the high objective value is reduced over time, after which the unrealistic temperature distribution disappears.

Finally, in order to show that the temperature difference between the terminal temperatures of a period and the initial temperatures of the subsequent period decreases, an optimisation test run has been setup. For this run, the maximum temperature difference between layers of two subsequent periods, $\Delta T_{m,n,\max}$, is monitored, which is defined as,

$$\Delta T_{m,n,\max} = \max\left(\left|T_{m,n,\text{init}} - T_{(m-1),n,\text{end}}\right|\right). \tag{B.12}$$

To work as designed, it should hold that $\Delta T_{m,n,\max}$, reduces for an increasing number of iterations. That this holds is observed in Figure B.3, where $\Delta T_{m,n,\max}$ is reduced to 0.059 [°C] after 150 iterations, thus matching the periods as designed.

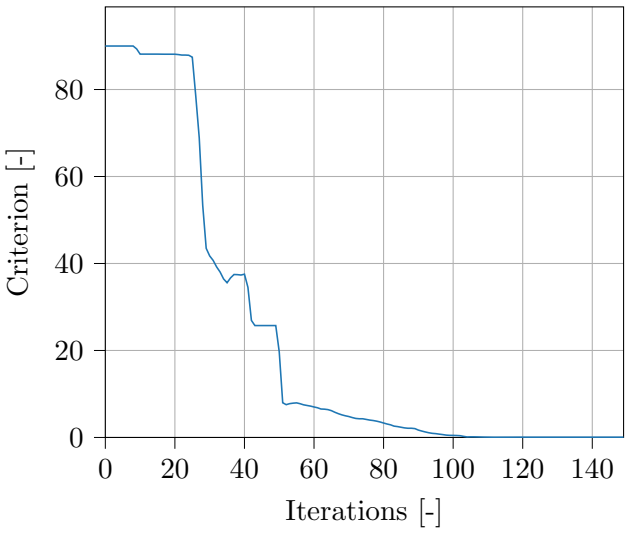

Figure B.3: The maximum temperature difference between two layers versus the number of iterations shows that the difference decreases with an increasing number of iterations.

To summarise, the model heats the tank at the expected time, puts a penalty on unrealistic temperature distributions, and decreases the temperature differences between periods. Therefore, it is concluded that the objective function behaves as expected.

B.4 Validation of CVXPY

To validate that CVXPY minimises a given objective function, it is desired that CVXPY is compared with an analytical solution. However, it is stated that convex optimisation problems generally do not have an analytical solution (Boyd & Vandenberghe, 2004). Nevertheless, there exists a special group of convex optimisation problems that does have an analytical solution, so-called least-squares optimisation problems. An unconstrained least-squares optimisation problem is of the form,

$$\text{minimise} \quad \|Ax - b\|_2^2, \tag{B.13}$$

where $A \in \mathbf{R}^{l \times p}$, $x \in \mathbf{R}^p$, and $b \in \mathbf{R}^l$.

Convexity of least-squares problems

To prove that least-squares problems are indeed convex, and therefore can be solved using CVXPY. It must hold that,

$$f(\theta\beta + (1-\theta)\,\gamma) \leq \theta f(\beta) + (1-\theta)\,f(\gamma), \tag{B.14}$$

$$f(\theta\beta + (1-\theta)\,\gamma) - \theta f(\beta) - (1-\theta)\,f(\gamma) \leq 0, \tag{B.15}$$

for all β, $\gamma \in \mathbf{R}^p$ and all $\theta \in [0, 1]$ (Diamond et al., 2020).

Rewriting the objective function of a least-squares problem as defined in Equation B.13 results in the equation,

$$f(x) = \frac{1}{2l}\,(Ax-b)^T\,(Ax-b)\,. \tag{B.16}$$

For convenience, the constant factor, $\frac{1}{2l}$, is omitted because multiplying the objective function with a constant does not affect the minimisation result, which reduces the objective function to,

$$\begin{aligned} f(x) &= (Ax-b)^T\,(Ax-b)\,, \\ &= \left((Ax)^T - b^T\right)(Ax-b)\,, \\ &= (Ax)^T\,(Ax) - (Ax)^T\,b - b^T\,(Ax) + b^T b, \\ &= x^T A^T A x - 2b^T A x + b^T b. \end{aligned} \tag{B.17}$$

Note that $(Ax-b)$ is affine due to its linearity and is derived in a similar way as presented in section B.1. Therefore, $2b^T Ax + b^T b$ reduces to zero. The remaining terms of $f(x)$ are substituted in Equation B.15, resulting in the following equations,

$$(\theta\beta + (1-\theta)\,\gamma)^T\,A^T A\,(\theta\beta + (1-\theta)\,\gamma) - \theta\beta^T A^T A\beta - (1-\theta)\,\gamma^T A^T A\gamma \leq 0, \tag{B.18}$$

$$\theta^2\beta^T A^T A\beta + (1-\theta)^2\,\gamma^T A^T A\gamma + 2\theta\,(1-\theta)\,\beta^T A^T A\gamma - \theta\beta^T A^T A\beta - (1-\theta)\,\gamma^T A^T A\gamma \leq 0, \tag{B.19}$$

with,

$$\beta^T A^T A\gamma = (A\beta)^T\,(A\gamma) = (A\gamma)^T\,(A\beta) = \gamma^T A^T A\beta, \tag{B.20}$$

then reduces Equation B.19 to,

$$\begin{aligned} \left(\theta^2-\theta\right)\beta^T A^T A\beta + \left((1-\theta)^2 - (1-\theta)\right)\gamma^T A^T A\gamma + 2\theta\,(1-\theta)\,\beta^T A^T A\gamma \leq 0, \\ -\theta\,(1-\theta)\left(\beta^T A^T A\beta + \gamma^T A^T A\gamma - 2\beta^T A^T A\gamma\right) \leq 0, \\ -\theta\,(1-\theta)\left(\beta^T A^T A\beta + \gamma^T A^T A\gamma - 2\beta^T A^T A\gamma\right) \leq 0, \\ -\theta\,(1-\theta)\left((\beta-\gamma)^T\,A^T A\,(\beta-\gamma)\right) \leq 0, \\ -\theta\,(1-\theta)\,\|A\,(\beta-\gamma)\,\|_2^2 \leq 0, \end{aligned} \tag{B.21}$$

which is proves that a least-squares optimisation problem is convex as $-\theta\,(1-\theta)\,\|A\,(\beta-\gamma)\,\|_2^2$ is always ≤ 0.

Analytical solution

It is stated that an analytical solution exist for least-square problems. To derive the analytical solution for Equation B.13, the residual, r, is introduced, which is defined as follows,

$$r = A\hat{x} - b, \tag{B.22}$$

with $\hat{x}$ the optimal x. If $\|r\|_2^2 = 0$, a perfect fit is obtained. Therefore, the optimisation problem becomes as follows,

$$\text{minimise} \quad \|r\|_2^2, \tag{B.23}$$

with,

$$\|r\|_2^2 = \|A\hat{x} - b\|_2^2 = (A\hat{x} - b)^T (A\hat{x} - b) = \hat{x}^T A^T A\hat{x} - 2b^T A\hat{x} + b^T b. \tag{B.24}$$

In order to obtain the minimum, the first derivative with respect to $\hat{x}$ should be equal to zero,

$$\begin{aligned} \frac{\partial f(\hat{x})}{\partial \hat{x}} = A^T A\hat{x} + A^T A\hat{x} - 2A^T b = 0, \\ 2A^T A\hat{x} - 2A^T b = 0. \end{aligned} \tag{B.25}$$

Rewriting results in the analytical solution denoted as follows,

$$\hat{x} = \left(A^T A\right)^{-1} A^T b. \tag{B.26}$$

Comparison between the analytical solution and CVXPY

It is established that least-squares problems are convex and can therefore be modelled using CVXPY. The modelled least-squares optimisation problem is compared to the analytical solution, presented in Equation B.26.

Solving the the optimisation problem in Equation B.13 for $l = 15$ and $p = 5$ with random dimensionless numbers, results in the objective value and solution vector as presented in Table B.1. This table also presents the analytical solution for the modelled least-squares problem. It is observed that the result obtained by using CVXPY and the analytical solution are nearly identical. To visualise this, $A_{l,4}x_4$ is compared with b in Figure B.4. Therefore, it is validated that CVXPY minimises a given objective function.

Table B.1: Analytical and CVXPY modelled solution for a least-squares optimisation problem.

	Objective function [-]	Optimal variable
Analytical	5.85917807	$\hat{x} = [0.44298833, 0.54382117, -0.43339320 , 0.47651026, 0.20809495]^T$
CVXPY	5.85917835	$x = [0.44298833, 0.54382117, -0.43339320 , 0.47651026, 0.20809495]^T$

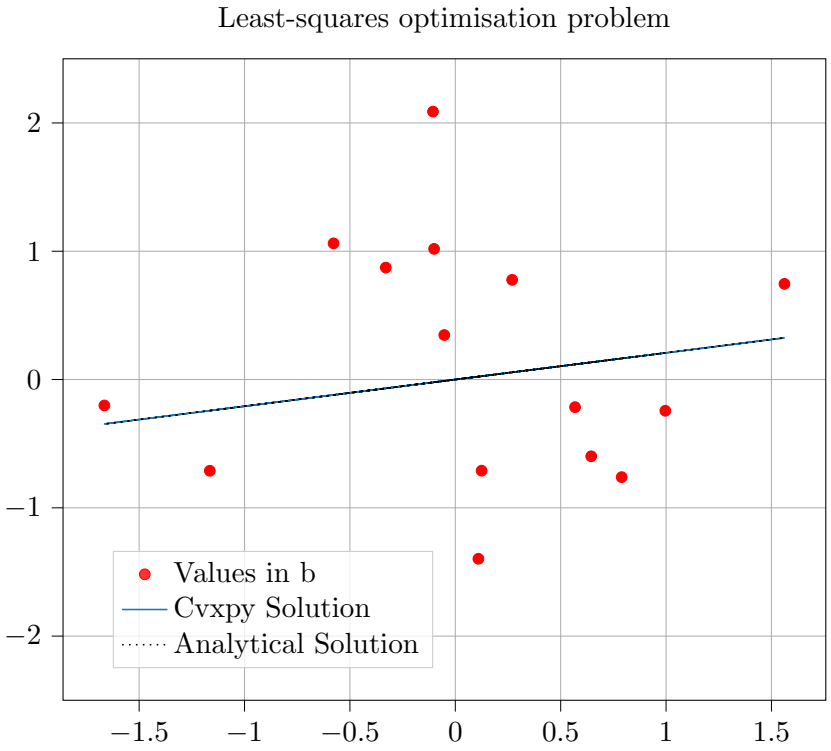

Figure B.4: Visualisation of the least-squares optimisation problem, comparing $A_{l,4}x_4$ with b. This figure shows that the solution obtained by using CVXPY is nearly equal to the analytical solution.

TU/e EINDHOVEN UNIVERSITY OF TECHNOLOGY

Declaration concerning the TU/e Code of Scientific Conduct for the Master's thesis

I have read the TU/e Code of Scientific Conduct[1].

I hereby declare that my Master's thesis has been carried out in accordance with the rules of the TU/e Code of Scientific Conduct

Date

October 7, 2020

Name

Margje van der Heuvel

ID-number

0950302

Signature

Submit the signed declaration to the student administration of your department.

[1] See: https://www.tue.nl/en/our-university/about-the-university/organization/integrity/scientific-integrity/
The Netherlands Code of Conduct for Scientific Integrity, endorsed by 6 umbrella organizations, including the VSNU, can be found here also. More information about scientific integrity is published on the websites of TU/e and VSNU